

Variational Inverting Network for Statistical Inverse Problems of Partial Differential Equations

Junxiong Jia

*School of Mathematics and Statistics,
Xi'an Jiaotong University,
Xi'an, 710049, China*

JJX323@MAIL.XJTU.EDU.CN

Yanni Wu

*School of Mathematics and Statistics,
Xi'an Jiaotong University,
Xi'an, 710049, China*

WUYANNI@STU.XJTU.EDU.CN

Peijun Li

*Department of Mathematics,
Purdue University,
West Lafayette, Indiana, 47907, USA*

LIPEIJUN@MATH.PURDUE.EDU

Deyu Meng*

*School of Mathematics and Statistics,
Xi'an Jiaotong University,
Xi'an, 710049, China;
Pazhou Lab, Guangzhou, 510330, China*

DYMENG@MAIL.XJTU.EDU.CN

Editor:

Abstract

To quantify uncertainties of the inverse problems governed by partial differential equations (PDEs), the inverse problems are transformed into statistical inference problems based on Bayes' formula. Recently, infinite-dimensional Bayesian analysis methods are introduced to give a rigorous characterization and construct dimension-independent algorithms. However, there are three major challenges for infinite-dimensional Bayesian methods: prior measures usually only behaves like regularizers (can hardly incorporate prior information efficiently); complex noises (e.g., more practical non-identically distributed noises) are rarely considered; many computationally expensive forward PDEs need to be solved in order to estimate posterior statistical quantities. To address these issues, we propose a general infinite-dimensional inference framework based on a detailed analysis on the infinite-dimensional variational inference method and the ideas of deep generative models that are popular in the machine learning community. Specifically, by introducing some measure equivalence assumptions, we derive the evidence lower bound in the infinite-dimensional setting and provide possible parametric strategies that yield a general inference framework named variational inverting network (VINet). This inference framework has the ability to encode prior and noise information from learning examples. In addition, relying on the power of deep neural networks, the posterior mean and variance can be efficiently generated in the inference stage in an explicit manner. In numerical experiments, we design specific network structures that yield a computable VINet from the general inference framework. Numerical

cal examples of linear inverse problems governed by an elliptic equation and the Helmholtz equation are given to illustrate the effectiveness of the proposed inference framework.

Keywords: Infinite-dimensional variational inference, inverse problems, Bayesian analysis for functions, partial differential equations, deep neural networks

1. Introduction

Motivated by their significant applications in seismic exploration, radar imaging, and many other domains, inverse problems for partial differential equations (IPfPDEs) have undergone an enormous development over the past few decades (Engl et al., 1996). As the computational power keeps increasing, researchers are not satisfied with obtaining just an estimated solution, but pursue to perform some statistical analysis based on uncertainty information, which is essential for some applications, such as artifact detecting (Zhou et al., 2020). The Bayesian inverse approach provides a flexible framework that solves inverse problems by transforming them into statistical inference problems (Stuart, 2010), thereby making it popular to analyze the uncertainties of the interested parameters in IPfPDEs.

As is known, partial differential equations (PDEs) are usually defined on some infinite-dimensional spaces of functions (Evans, 2010), which introduce difficulties to the direct use of the finite-dimensional Bayes' formula. To resolve this issue, a straightforward way is to use discretized PDEs to approximate the original problem in some finite-dimensional spaces and solve the reduced approximate problems by certain finite-dimensional Bayes' methods. This strategy makes nearly all of the parametric Bayesian inference methods developed in the statistical literatures available (Berger, 1980; Kaipio and Somersalo, 2005). Especially, under the finite-dimensional (FD) setting, machine learning methods, e.g., Wasserstein GAN (Adler and Öktem, 2018), have been recently employed to learn the prior and construct fast sampling algorithms. However, given the original problems defined on the infinite-dimensional (ID) space, some critical issues are inevitably encountered:

1. Model consistency: The elements in a finite-dimensional model (e.g., prior probability measure) possess different intrinsic characteristics from its intuitive infinite-dimensional counterparts. One typical example is the total variation prior measure, which has been comprehensively analyzed in (Lassas and Siltanen, 2004).
2. Algorithm applicability: Discrete quantities in IPfPDEs are expected to converge to functions belong to some ID spaces. Under the FD setting, however, we still lack rigorously defined inference algorithm on ID space, which prevents the usage of the powerful tools in numerical analysis.
3. Sampling efficiency: For typical Markov chain Monte Carlo (MCMC) algorithm defined on finite-dimensional spaces, sample efficiency from the posterior measure inclines to be largely dropped when the dimension of the parameters increases (Cotter et al., 2013).

For overcome these obstacles, Bayes' formula defined on some separable Banach space is employed to handle IPfPDEs (Dashti and Stuart, 2017; Stuart, 2010), which can be seen as a recently emerging research topic in the field of the nonparametric Bayesian inference

approach. We refer to (Ghosal and Vaart, 2017) for general investigations on the nonparametric Bayesian inference approach. Beyond the IPfPDEs field, Bayes’ methods in ID spaces have also been employed to design new machine learning algorithms (Kovachki and Stuart, 2019) and perform theoretical analysis in recent years. The theory of well-posedness of ID Bayesian analysis method has been generalized to incorporate some machine learning problems (Latz, 2020). Relying on the ID Bayesian analysis theory, the graph-based Bayesian semi-supervised learning algorithms have been analyzed from some aspects, e.g., large data and zero noise limit (Dunlop et al., 2020), as well as consistency and scalability of sampling algorithms (Hoffmann et al., 2020; Trillos et al., 2020). ID Bayesian inference method proposed for IPfPDEs has been validated to be useful for some machine learning problems, and machine learning techniques could also be helpful for generalizing ID Bayesian theory. Generally speaking, there are three main research directions for ID Bayesian analysis methods: designing prior probability measures on ID space, constructing appropriate noise models, and extracting information from posterior measures with efficiency. In the following, we review some typical works along the above three research directions, as well as illustrate their intrinsic issues in applications.

Concerned with prior measures defined on the ID space, Gaussian measure is very popular based on its abundant theoretical studies in the field of stochastic PDEs (Prato and Zabczyk, 2014). Related studies on employing Gaussian prior measures can be found in (Agapiou et al., 2014; Bui-Thanh et al., 2013; Bui-Thanh and Nguyen, 2016; Cotter et al., 2009; Jia et al., 2021c; Wang et al., 2018). To characterize the discontinuity of the function parameters, the Besov type prior measure has been proposed (Lassas et al., 2009; Dashti et al., 2012; Jia et al., 2016). Recently, the well-posedness of the Bayesian inverse method under prior measures with exponential tails has been analyzed in (Hosseini and Nigam, 2017). Besides, starting from the seminal work (Knapik et al., 2011), the posterior consistency and contraction rates have been analyzed in details in a series of works (Agapiou et al., 2013; Giordano and Nickl, 2020; Jia et al., 2021b; Kekkonen et al., 2016; Szabó et al., 2015; Vollmer, 2013), which convey a general understanding of what types of priors make a Bayesian nonparametric method effective. However, as illustrated in (Adler and Öktem, 2018; Arridge et al., 2019), most of these priors need to be pre-designed by hand-craft, and thus always not sufficient and flexible enough to describe intrinsic characteristics underlying the investigated problem. This makes these priors more often chosen as a regularizer rather than essentially improve the quality of the final output (Arridge et al., 2019). Thus it is desirable to adaptably encode a prior specifically suitable for a certain input by data-driven manners (Adler and Öktem, 2018).

For the noise model, the Gaussian measure is also frequently used in the research literature, e.g., Gaussian noise setting is employed in (Bui-Thanh et al., 2013; Bui-Thanh and Nguyen, 2016; Jia et al., 2018; Wang et al., 2018). By characterizing the model error as a Gaussian random variable, a Bayesian method with approximate error can then be constructed (Kaipio and Somersalo, 2005). A natural generalization has been proposed in (Jia et al., 2019), which employed a mixture of Gaussian (MoG) distributions to characterize model noises to make it a better fit for a wider range of noise types due to the universe approximation capability of MoG for general distributions. Through a learning process, the model error information has been encoded into the parameters of Gaussian mixture distributions, which improves the estimate quality by only using an approximate forward

solver. However, the method proposed in (Jia et al., 2019) only provide maximum a posterior (MAP) estimate, which can be seen as an incomplete Bayesian approach. Besides, they still have not considered more general and practical non-independently and non-identically distributed (non-i.i.d) noises.

Extracting information from the posterior measure is one of the essential issues for employing the Bayes' method. Sampling algorithms, such as MCMC, are often employed. The preconditioned Crank–Nicolson algorithm defined on some infinite-dimensional space has been proposed (Cotter et al., 2013) to ensure the robustness of the convergence speed under mesh refinement. Then, multiple dimension-independent MCMC-type sampling algorithms have been proposed (Agapiou et al., 2017; Beskos et al., 2015; Cui et al., 2016; Feng and Li, 2018). However, as illustrated in (Arridge et al., 2019), the current sampling algorithms still face the critical issue of computational efficiency, especially for large-scale inverse problems.

Under the finite-dimensional (FD) setting, the variational inference (VI) methods have been broadly investigated in machine learning (Zhang et al., 2018) to reduce the computational burden of MCMC-type sampling algorithms. Compared with the FD problems, the ID problems are much less studied for the VI methods. When the approximate measures are restricted to be Gaussian, the novel Robbins-Monro algorithm was developed in (Pinski et al., 2015a,b) from a calculus-of-variations viewpoint. It was shown in (Sun et al., 2019) that the Kullback-Leiber (KL) divergence between the stochastic processes is equal to the supremum of the KL divergence between the measures restricted to finite marginals. Meanwhile, they developed a VI method for functions parameterized by Bayesian neural networks. Under the classical mean-field assumption, a general VI framework defined on separable Hilbert space was proposed recently in (Jia et al., 2021c). A function space particle optimization method including the Stein variational gradient descent (SVGD) was developed in (Wang et al., 2019) to solve the particle optimization directly in the space of functions. SVGD with preconditioning operators has further been proposed in (Jia et al., 2021a), which provides a detailed mathematical analysis in some separable Hilbert space. These VI methods defined on ID space have been proposed to train deep neural networks (DNNs) or solve IPfPDEs, which indeed ameliorate the computational complexity to a certain extent. However, for solving IPfPDEs, many forward and adjoint PDEs are still need to be solved, which is time-consuming. Furthermore, as illustrated in (Arridge et al., 2019), these VI methods also require to manually pre-design priors with explicit forms, which is always not sufficiently flexible and adaptable to faithfully deliver complicated prior knowledge underlying the investigated problem.

Through the above review and discussions, we summarize the main points as follows:

1. To more efficiently and adaptably encode prior information (not just for regularizing), machine learning methods with data-driven manners are expected to be involved into the ID setting.
2. MoG noise modeling strategies have been introduced to improve the noise fitting capability of the problem by current research, but they are still restrictive on i.i.d. noise types while more practical non-i.i.d. noise cases are more expected to be considered.
3. Although infinite-dimensional VI (IDVI) methods have been proposed recently, time-consuming iterations are still inevitably required. More efficient regimes are thus

required to be investigated. Besides, it is highly expected for current IDVI methods to flexibly and faithfully specify priors directly from data rather than commonly adopted hand-crafted manners.

To address these issues, inspired by recent investigations on image denoising and restorations (Yue et al., 2019, 2020), we propose a general IDVI method that intends to integrate the prior information learning, noise distribution learning, and posterior mean and covariance learning into a unified machine learning framework. In this work, we focus on linear inverse problems. For nonlinear problems, it is reasonable to consider the linearized problems (Jin and Zou, 2010). The noises of data are assumed to be non-i.i.d in statistics. For the prior measure, it is a little more complex. We presume that the synthetic background truth is acquired during the learning stage, which is obviously not available during the inverse computational stage (only the noisy data is available). The prior measure is assumed to be a Gaussian measure with synthetic background truth as the mean function. Under this setting, the posterior measure cannot be obtained during the inverse computational stage under the classical VI framework since the synthetic background truth involved in the prior measure is not available. Relying on the ideas of the generative model studied in the machine learning community (Kingma, 2017; Yue et al., 2019, 2020), we design an appropriate parameterized posterior measure by virtue of techniques of deep neural networks (DNNs). Through encoding the noise distribution information and prior information into the parameters of neural networks, the synthetic background truth will not be needed in the inverse computational stage. Intuitively, the inaccessible synthetic background truth in the inverse computational stage is replaced by the prior information directly learned from the training data. Numerical examples are given to illustrate the flexibility and effectiveness of the proposed approach.

In summary, this work mainly contains four contributions:

1. Inspired by the investigations on generative models in the FD setting (Kingma, 2017; Yue et al., 2019, 2020), we propose a general Bayesian generative model on ID space named as **V**ariational **I**nverting **N**etwork (VINet), which is naturally derived from the analysis on the IDVI method for linear inverse problems with non-i.i.d noises. Due to the general assumptions on the noises and priors, the proposed VINet integrates noise distribution learning, prior information learning, and posterior statistical estimation into a unified machine learning framework.
2. Instead of only focusing on the interested function parameters as conventional works like deep learning for elastic source imaging (Yoo et al., 2018) and deep Bayesian inversion (Adler and Öktem, 2018), the proposed VINet provides uncertainty information both on the function parameters and on the random noises. Thus, the noise and function parameter estimations can be mutually ameliorated during the inverse computational stage.
3. By imposing equivalence conditions on the prior and the approximate posterior measure, we derive the evidence lower bound (ELBO) under the ID setting. Then, we design an amortized variational inference method to guide the training of all variables involved in the proposed generative model. The model can then be explicitly used to achieve the posterior information of any noisy data without the time-consuming

iteration process and any prior and noise pre-assumptions. Thus, the model can more efficiently make inference for the IPfPDEs as compared with the conventional paradigms illustrated in (Dashti and Stuart, 2017).

4. We provide a specific parametric strategy by DNNs, which has been proved to satisfy the requirements of the general inference theory. Based on the proposed parametric strategy and the general abstract theory, we design a rational specific structure of VINet. Two numerical examples of typical IPfPDEs are given, substantiating the effectiveness of the proposed method.

The remainder of the paper is organized as follows. In Section 2, the general theory is presented. Specifically, in Subsection 2.1, the general settings of the employed Bayesian inference model is given. In Subsection 2.2, the Bayesian inference model is analyzed under the mean-field based infinite-dimensional VI framework. In Subsection 2.3, we construct the general Bayesian generative model (i.e., VINet), derive the amortized variational inference method, and provide a simple preliminary theoretical analysis. In Subsection 2.4, we introduce a specific parametric strategy that can parameterize the posterior. In Section 3, two numerical examples are given to illustrate the effectiveness of the proposed method. In particular, in Subsection 3.1, we design a specific network structure according to our general theory, and then apply the proposed VINet to a simple toy smoothing model in Subsection 3.2. We then demonstrate a more realistic example that is an inverse source problem governed by the Helmholtz equation in Subsection 3.3. In Section 4, we summarize our results and propose some directions for future research.

2. Variational Inverting Network

In this section, we construct the general inference model. A detailed analysis is then given for the Bayesian inference model under the mean-field based infinite-dimensional VI framework (Jia et al., 2021c). Afterwards, the general VINet framework is presented, the amortized variational inference method is introduced, a preliminary theoretical analysis is examined, and some parametric strategies are also discussed.

2.1 The Bayesian inference method

Let \mathcal{H}_u be a separable Hilbert space, N_d be a positive integer, and $H : \mathcal{H}_u \rightarrow \mathbb{R}^{N_d}$ be a bounded linear operator. Consider the problem

$$\mathbf{d} = Hu + \boldsymbol{\epsilon}, \quad (2.1)$$

where \mathbf{d} and $\boldsymbol{\epsilon} \in \mathbb{R}^{N_d}$ represent the measurement data and the random noise, respectively. Denote by \mathcal{C}_0 the symmetric, positive definite, and trace class operator defined on \mathcal{H}_u . Let (e_k, α_k) be an eigen-system of the operator \mathcal{C}_0 such that $\mathcal{C}_0 e_k = \alpha_k e_k$. Without loss of generality, we assume that the eigenvectors $\{e_k\}_{k=1}^{\infty}$ are orthonormal and the eigenvalues $\{\alpha_k\}_{k=1}^{\infty}$ are sorted in a descending order. It follows from Subsection 2.4 in (Dashti and Stuart, 2017) that we have

$$\mathcal{C}_0 = \sum_{k=1}^{\infty} \alpha_k e_k \otimes e_k. \quad (2.2)$$

For the parameter u and the noise ϵ , we assume

$$u \sim \mu_0^u := \mathcal{N}(\bar{u}_0, \mathcal{C}_0), \quad \epsilon \sim \mathcal{N}(0, \Sigma), \quad (2.3)$$

where $\Sigma = \text{diag}(\sigma_1, \sigma_2, \dots, \sigma_{N_d})$ with $\{\sigma_i\}_{i=1}^{N_d}$ being a series of positive real numbers. Here, $\mathcal{N}(v, \mathcal{C})$ stands for a Gaussian measure with mean v and covariance operator \mathcal{C} . Clearly, $\mathcal{N}(\bar{u}_0, \mathcal{C}_0)$ denotes a Gaussian measure defined on \mathcal{H}_u with mean $\bar{u}_0 \in \mathcal{H}_u$ and covariance operator \mathcal{C}_0 , and $\mathcal{N}(0, \Sigma)$ is a Gaussian measure defined on \mathbb{R}^{N_d} .

For the additive noise model (2.1), the data \mathbf{d} are distributed according to the following translated distribution of ϵ :

$$\mathbf{d} \sim \mathcal{N}(Hu, \Sigma). \quad (2.4)$$

Usually, we assume that Σ is known a priori when making inferences on the ID parameter u . However, similar to such studies as in (Dunlop et al., 2017; Jin and Zou, 2010), we assume that the parameters $\{\sigma_i\}_{i=1}^\infty$ are unknown random variables, which are called hyper-parameters and also need to be estimated. The key elements of an abstract inverse problem can then be summarized as follows.

- **Noisy data:** The data vector $\mathbf{d} \in \mathbb{R}^{N_d}$ is obtained from $\mathbf{d} = Hu^\dagger + \epsilon$, where u^\dagger is the background truth and $\epsilon \sim \mathcal{N}(0, \Sigma)$ with $\Sigma = \text{diag}(\sigma_1, \dots, \sigma_{N_d})$;
- **Inverse problem:** Based on the noisy data \mathbf{d} , the goal is to find estimates of u and the hyper-parameters $\boldsymbol{\sigma} := \{\sigma_1, \dots, \sigma_{N_d}\}$.

We assume that the hyper-parameters in Σ satisfy

$$\boldsymbol{\sigma} \sim \mu_0^\sigma := \prod_{i=1}^{N_d} \text{IG}(\alpha_i^0, \beta_i^0), \quad (2.5)$$

where $\alpha_i^0 > 1$ and $\beta_i^0 > 0$ ($i = 1, \dots, N_d$) are hyper-parameters that will be specified in numerical examples, and $\text{IG}(\alpha_i^0, \beta_i^0)$ denotes the inverse Gamma distribution with parameters α_i^0 and β_i^0 ($i = 1, \dots, N_d$).

Now, a Bayes' formulation can be constructed for the corresponding linear inverse problem. We introduce the prior probability measure

$$\mu_0 := \mu_0^u \otimes \mu_0^\sigma. \quad (2.6)$$

Let

$$\Phi(u, \boldsymbol{\sigma}; \mathbf{d}) := \frac{1}{2} \|\mathbf{d} - Hu\|_\Sigma^2 + \frac{1}{2} \log(\det \Sigma), \quad (2.7)$$

where $\|\cdot\|_\Sigma := \|\Sigma^{-1/2} \cdot\|$ and $\det \Sigma$ is the determinant of Σ . Since H is a bounded linear operator, it is easy to deduce that $\Phi(u, \boldsymbol{\sigma}; \mathbf{d})$ is continuous with respect to the variables u , $\boldsymbol{\sigma}$, and \mathbf{d} . Following simple calculations, we have

$$\Phi(u, \boldsymbol{\sigma}; \mathbf{d}) = \frac{1}{2} \|\mathbf{d} - Hu\|_\Sigma^2 + \frac{1}{2} \log(\det \Sigma) \geq \frac{1}{2} \log \left(\prod_{k=1}^{N_d} \sigma_k \right) = \frac{1}{2} \sum_{k=1}^{N_d} \log(\sigma_k) \quad (2.8)$$

and

$$\begin{aligned}
 |\Phi(u, \boldsymbol{\sigma}; \mathbf{d}_1) - \Phi(u, \boldsymbol{\sigma}; \mathbf{d}_2)| &= ||\mathbf{d}_1 - Hu||_{\Sigma} - ||\mathbf{d}_2 - Hu||_{\Sigma}| \\
 &\leq \|\Sigma^{-1/2}(\mathbf{d}_1 - \mathbf{d}_2)\| \\
 &\leq \sum_{k=1}^{N_d} \frac{1}{\sigma_k^{1/2}} \|\mathbf{d}_1 - \mathbf{d}_2\|.
 \end{aligned} \tag{2.9}$$

Noting

$$\exp\left(\sum_{k=1}^{N_d} \log \sigma_k\right) = \prod_{k=1}^{N_d} \sigma_k \in L_{\mu_0}^1(\mathcal{H}_u \times \mathbb{R}^+; \mathbb{R}) \tag{2.10}$$

and

$$\exp\left(\sum_{k=1}^{N_d} \log \sigma_k\right) \left(\sum_{k=1}^{N_d} \frac{1}{\sigma_k^{1/2}}\right)^2 \leq \sum_{k=1}^{N_d} \left(\prod_{i=1, i \neq k}^{N_d} \sigma_i\right) \in L_{\mu_0}^1(\mathcal{H}_u \times \mathbb{R}^+; \mathbb{R}), \tag{2.11}$$

we know that Assumption 1 and the conditions of Theorems 15–16 in (Dashti and Stuart, 2017) are satisfied, which provide the following Bayes formula defined on ID space:

$$\frac{d\mu^{\mathbf{d}}}{d\mu_0}(u, \boldsymbol{\sigma}) = \frac{1}{Z_{\mathbf{d}}} \det(\Sigma)^{-1/2} \exp\left(-\frac{1}{2}\|\mathbf{d} - Hu\|_{\Sigma}^2\right), \tag{2.12}$$

where $\mu^{\mathbf{d}}$ represents the posterior probability measure and

$$Z_{\mathbf{d}} = \int_{(\mathbb{R}^+)^{N_d}} \int_{\mathcal{H}_u} \det(\Sigma)^{-1/2} \exp\left(-\frac{1}{2}\|\mathbf{d} - Hu\|_{\Sigma}^2\right) \mu_0^u(du) \mu_0^{\boldsymbol{\sigma}}(d\boldsymbol{\sigma}). \tag{2.13}$$

2.2 The infinite-dimensional variational inference method

Before constructing the VINet, we discuss the mean-field assumption based ID variational inference (IDVI) theory developed in (Jia et al., 2021c). A brief introduction is given in Subsection 5.1 of Appendix.

In Subsection 2.1, we have not introduced hyper-parameters involved in the prior probability measure. Hence, we can choose the prior measure μ_0 as the reference probability measure required in Assumption 8 in (Jia et al., 2021c). Using the mean-field approximation, i.e., assuming the parameters u and $\boldsymbol{\sigma}$ to be independent random variables, we introduce an approximate probability measure $\nu(du, d\boldsymbol{\sigma}) = \nu^u(du)\nu^{\boldsymbol{\sigma}}(d\boldsymbol{\sigma})$ with

$$\frac{d\nu^u}{d\mu_0^u}(u) = \frac{1}{Z_u} \exp(-\Phi_u(u)) \tag{2.14}$$

and

$$\frac{d\nu^{\boldsymbol{\sigma}}}{d\mu_0^{\boldsymbol{\sigma}}}(\boldsymbol{\sigma}) = \frac{1}{Z_{\boldsymbol{\sigma}}} \exp(-\Phi_{\boldsymbol{\sigma}}(\boldsymbol{\sigma})), \tag{2.15}$$

where $\Phi_u(\cdot)$ and $\Phi_\sigma(\cdot)$ are two potential functions required to be calculated explicitly, and

$$Z_u = \mathbb{E}^{\mu_u^0} [\exp(-\Phi_u(u))], \quad Z_\sigma = \mathbb{E}^{\mu_\sigma^0} [\exp(-\Phi_\sigma(\sigma))].$$

Here, \mathbb{E}^μ represents taking expectation with respect to the probability measure μ .

The VI method essentially needs to solve the optimization problem

$$\arg \min_{\nu^u \in \mathcal{A}_u, \nu^\sigma \in \mathcal{A}_\sigma} D_{\text{KL}}(\nu || \mu^d), \quad (2.16)$$

where \mathcal{A}_u and \mathcal{A}_σ are two appropriate spaces of probability measure, and $D_{\text{KL}}(\nu || \mu^d)$ is the Kullback-Leibler (KL) divergence defined as follows:

$$D_{\text{KL}}(\nu || \mu^d) = \int_{\mathcal{H}} \log \left(\frac{d\nu}{d\mu^d}(x) \right) \frac{d\nu}{d\mu^d}(x) \mu^d(dx) = \mathbb{E}^{\mu^d} \left[\log \left(\frac{d\nu}{d\mu^d}(x) \right) \frac{d\nu}{d\mu^d}(x) \right].$$

Here $0 \log 0 = 0$ is used as conventional. For the finite-dimensional theory (e.g., Chapter 10 in (Bishop, 2006)), it is not needed to add additional assumptions on \mathcal{A}_u and \mathcal{A}_σ . However, we need to pay special attention to \mathcal{A}_u and \mathcal{A}_σ in the infinite-dimensional theory (Jia et al., 2021c).

Define $T_N^u = \{u \mid 1/N \leq \|u\|_{\mathcal{Z}_u} \leq N\}$ with \mathcal{Z}_u being a Hilbert space that is embedded in \mathcal{H}_u and satisfies $\sup_N \mu_0^u(T_N^u) = 1$. Denote $T_N^\sigma = \{\sigma \mid 1/N \leq \sigma_i \leq N \text{ for } i = 1, \dots, N_d\}$ that obviously satisfies $\sup_N \mu_0^\sigma(T_N^\sigma) = 1$. Let

$$R_u^1 = \left\{ \Phi_u \mid \sup_{u \in T_N^u} \Phi_u(u) < \infty \text{ for all } N > 0 \right\},$$

$$R_u^2 = \left\{ \Phi_u \mid \int_{\mathcal{H}_u} \exp(-\Phi_u(u)) \max(1, \|u\|_{\mathcal{H}_u}^2) \mu_0^u(du) < \infty \right\},$$

$$R_\sigma^1 = \left\{ \Phi_\sigma \mid \sup_{\sigma \in T_N^\sigma} \Phi_\sigma(\sigma) < \infty \text{ for all } N > 0 \right\},$$

$$R_\sigma^2 = \left\{ \Phi_\sigma \mid \int_{(\mathbb{R}^+)^{N_d}} \exp(-\Phi_\sigma(\sigma)) \max(1, a(\epsilon, \sigma)) \mu_0^\sigma(d\sigma) < \infty, \text{ for } \epsilon \in [0, \epsilon_0] \right\},$$

where $a(\epsilon, \sigma) := \sum_{i=1}^{N_d} \max(\sigma_i^\epsilon, \exp(\epsilon/\sigma_i))$ and ϵ_0 is a fixed positive number. Usually, we may choose $\epsilon_0 \ll \min_{1 \leq i \leq N_d} \{\alpha_i^0, \beta_i^0\}$ with $\{\alpha_i^0, \beta_i^0\}_{i=1}^{N_d}$ as introduced in (2.5). Define

$$\mathcal{A}_u = \left\{ \nu^u \in \mathcal{M}(\mathcal{H}_u) \mid \begin{array}{l} \nu^u \text{ is equivalent to } \mu_0^u \text{ with (2.14) holding true,} \\ \text{and } \Phi_u \in R_u^1 \cap R_u^2 \end{array} \right\},$$

$$\mathcal{A}_\sigma = \left\{ \nu^\sigma \in \mathcal{M}(\mathcal{H}_\sigma) \mid \begin{array}{l} \nu^\sigma \text{ is equivalent to } \mu_0^\sigma \text{ with (2.15) holding true,} \\ \text{and } \Phi_\sigma \in R_\sigma^1 \cap R_\sigma^2 \end{array} \right\}.$$

Remark 1 The definitions of R_u^1 and R_σ^1 are slightly different from the corresponding definitions of R_j^1 ($j = 1, \dots, M$) provided in (Jia et al., 2021c). The sets R_k^1 ($k = u, \sigma$) defined here enlarge the original definition (without uniform bound), which makes the theory more appropriate. For completeness, we provide a short illustration of the modified general theory in Subsection 5.1 of Appendix.

Next, we present the key theorem, which leads to an iterative algorithm.

Theorem 2 Assume that the prior measure μ_0 , noise measure, and posterior measure are defined in (2.6), (2.5), and (2.12), respectively. Let $\Phi(u, \sigma; \mathbf{d})$ be defined in (2.7). If \mathcal{A}_u and \mathcal{A}_σ are defined as above, then the problem (2.16) possesses a solution $\nu(du, d\sigma) = \nu^u(du)\nu^\sigma(d\sigma)$, which satisfies

$$\frac{d\nu}{d\mu_0}(u, \sigma) \propto \exp(-\Phi_u(u) - \Phi_\sigma(\sigma)), \quad (2.17)$$

where

$$\Phi_u(u) = \int_{(\mathbb{R}^+)^{N_d}} \Phi(u, \sigma; \mathbf{d}) \nu^\sigma(d\sigma) + \text{Const}, \quad (2.18)$$

$$\Phi_\sigma(\sigma) = \int_{\mathcal{H}_u} \Phi(u, \sigma; \mathbf{d}) \nu^u(du) + \text{Const}. \quad (2.19)$$

Here, “Const” denotes some general constant. Furthermore, we have

$$\nu^u(du) \propto \exp(-\Phi_u(u)) \mu_0^u(du), \quad \nu^\sigma(d\sigma) \propto \exp(-\Phi_\sigma(\sigma)) \mu_0^\sigma(d\sigma).$$

To avoid a possible distraction from the presentation of the work, the proof of this theorem is given in Subsection 5.2 of Appendix. In the following, we denote $\Phi(u, \sigma)$ instead of $\Phi(u, \sigma; \mathbf{d})$ when there are no ambiguities from the context.

Remark 3 In the general theory, the space of parameters is assumed to be a separable Hilbert space. The parameter σ resides in $(\mathbb{R}^+)^{N_d}$ which is not a Hilbert space. However, as stated in Remark 15 in (Jia et al., 2021c), a simple transformation can be adopted, e.g., $\sigma'_k = \log \sigma_k$ ($k = 1, \dots, N_d$). Then the new parameter $\sigma' = \{\sigma'_1, \dots, \sigma'_{N_d}\}$ belongs to \mathbb{R}^{N_d} , which is a Hilbert space. All of the statements and verification of σ can be equivalently transformed to the new variable σ' . Hence, we still use the parameter σ . With this slightly abuse use of the general theory, which can be rigorously verified through the above simple transformation, the reader may intuitively know the connection between the finite- and infinite-dimensional theories.

Using Theorem 2, we can then present a classical iterative algorithm when the parameter u belongs to some infinite-dimensional separable Hilbert space \mathcal{H}_u .

Calculate $\Phi_u(u)$. A direct application of (2.18) yields

$$\begin{aligned} \Phi_u(u) &= \frac{1}{2} \int_{(\mathbb{R}^+)^{N_d}} \left(\|\mathbf{d} - Hu\|_\Sigma^2 + \sum_{k=1}^{N_d} \log \sigma_k \right) \nu^\sigma(d\sigma) + \text{Const} \\ &= \frac{1}{2} \int_{(\mathbb{R}^+)^{N_d}} (\mathbf{d} - Hu)^T \Sigma^{-1} (\mathbf{d} - Hu) \nu^\sigma(d\sigma) + \text{Const}. \end{aligned} \quad (2.20)$$

Denoting

$$\Sigma_{\text{inv}}^* = \text{diag} \left(\mathbb{E}^{\nu^\sigma} [\sigma_1^{-1}], \dots, \mathbb{E}^{\nu^\sigma} [\sigma_{N_d}^{-1}] \right), \quad (2.21)$$

we have

$$\Phi_u(u) = \frac{1}{2} \|\mathbf{d} - Hu\|_{\Sigma_{\text{inv}}^*}^2 + \text{Const}. \quad (2.22)$$

Hence,

$$\frac{d\nu^u}{d\mu_0^u}(u) \propto \exp \left(-\frac{1}{2} \|\mathbf{d} - Hu\|_{\Sigma_{\text{inv}}^*}^2 \right), \quad (2.23)$$

which implies that the approximate posterior measure of u is a Gaussian measure

$$\nu^u = \mathcal{N}(\bar{u}_p, \mathcal{C}_p), \quad (2.24)$$

where

$$\mathcal{C}_p^{-1} = H^* \Sigma_{\text{inv}}^* H + \mathcal{C}_0^{-1}, \quad \bar{u}_p = \mathcal{C}_p (H^* \Sigma_{\text{inv}}^* \mathbf{d} + \mathcal{C}_0^{-1} \bar{u}_0). \quad (2.25)$$

Calculate $\Phi_\sigma(\sigma)$. Following (2.19), we have

$$\begin{aligned} \Phi_\sigma(\sigma) &= \frac{1}{2} \int_{\mathcal{H}_u} \left(\|\mathbf{d} - Hu\|_{\Sigma}^2 + \sum_{k=1}^{N_d} \log \sigma_k \right) \nu^u(du) + \text{Const} \\ &= \frac{1}{2} \int_{\mathcal{H}_u} (\mathbf{d} - Hu)^T \Sigma^{-1} (\mathbf{d} - Hu) \nu^u(du) + \frac{1}{2} \sum_{k=1}^{N_d} \log \sigma_k + \text{Const} \\ &= \sum_{k=1}^{N_d} \frac{1}{2} \left(\int_{\mathcal{H}_u} (d_k - (Hu)_k)^2 \nu^u(du) \frac{1}{\sigma_k} + \log \sigma_k \right) + \text{Const}. \end{aligned} \quad (2.26)$$

Hence,

$$\frac{d\nu^\sigma}{d\mu_0^\sigma}(\sigma) \propto \exp \left(-\sum_{k=1}^{N_d} \frac{1}{2} \left(\mathbb{E}^{\nu^u} [(d_k - (Hu)_k)^2] \frac{1}{\sigma_k} + \log \sigma_k \right) \right). \quad (2.27)$$

Recalling

$$\mu_0^\sigma(d\sigma) \propto \prod_{k=1}^{N_d} \sigma_k^{-\alpha_k^0 - 1} \exp \left(-\frac{\beta_k^0}{\sigma_k} \right) d\sigma, \quad (2.28)$$

we obtain

$$\nu^\sigma(d\sigma) \propto \prod_{k=1}^{N_d} \sigma_k^{-\alpha_k^0 - \frac{3}{2}} \exp \left(-\frac{\beta_k^0 + \frac{1}{2} \mathbb{E}^{\nu^u} [(d_k - (Hu)_k)^2]}{\sigma_k} \right) d\sigma, \quad (2.29)$$

which implies that the posterior distribution of each component of ν^σ is of the following form:

$$\sigma_k \sim \text{IG} \left(\alpha_k^0 + \frac{1}{2}, \beta_k^0 + \frac{1}{2} \mathbb{E}^{\nu^u} [(d_k - (Hu)_k)^2] \right), \quad k = 1, \dots, N_d. \quad (2.30)$$

The above illustrations confirm the feasibility of Algorithm 1, which is similar to the finite-dimensional case. However, it is worth mentioning that the infinite-dimensional formulation provides a general framework for conducting appropriate discretizations. To keep dimension independent properties, the discretization of Algorithm 1 should be done carefully, e.g., the adjoint operator H^* is usually not trivially equal to the transpose of the discrete approximation of H . Please refer to (Jia et al., 2021c; Bui-Thanh et al., 2013; Petra et al., 2014; Wang et al., 2018; Bui-Thanh and Nguyen, 2016) for more detailed discussions on this topic. The infinite-dimensional formulation is well indicated by a recent study on the Stein variational gradient descent algorithm which is designed on the functional space for training DNNs (Wang et al., 2019).

Algorithm 1 A classical VI algorithm

- 1: Give an initial guess μ_0 (\bar{u}_0 , \mathcal{C}_0 , p , and $\{\alpha_i^0, \beta_i^0\}_{i=1}^{N_d}$). Specify the tolerance tol and set $k = 1$.
- 2: **repeat**
- 3: Set $k = k + 1$
- 4: Calculate Σ_{inv}^{k*} by $\mathbb{E}^{\nu_{k-1}^\sigma}[\sigma_i^{-1}] (i = 1, \dots, N_d)$
- 5: Calculate ν_k^u by

$$\mathcal{C}_p^{-1} = H^* \Sigma_{\text{inv}}^{k*} H + \mathcal{C}_0^{-1}, \quad u_k = \mathcal{C}_p (H^* \Sigma_{\text{inv}}^{k*} \mathbf{d} + \mathcal{C}_0^{-1} \bar{u}_0)$$

- 6: Calculate ν_k^σ by

$$\nu_k^\sigma = \prod_{i=1}^{N_d} \text{IG}(\alpha_i^k, \beta_i^k),$$

where

$$\alpha_i^k = \alpha_i^0 + \frac{1}{2}, \quad \beta_i^k = \beta_i^0 + \frac{1}{2} \mathbb{E}^{\nu_k^u} [(d_i - (Hu_k)_i)^2]$$

- 7: **until** $\max(\|u_k - u_{k-1}\|/\|u_k\|, \|\sigma_k - \sigma_{k-1}\|/\|\sigma_k\|) \leq tol$
 - 8: Return $\nu_k^u(du)\nu_k^\sigma(d\sigma)$ as the solution.
-

Remark 4 In the implementation of Algorithm 1, it is required to calculate $\mathbb{E}^{\nu_k^u} [(d_i - (Hu_k)_i)^2]$ for each $i = 1, \dots, N_d$. Regarding these terms, we have

$$\begin{aligned} \mathbb{E}^{\nu_k^u} [(d_i - (Hu_k)_i)^2] &= \int (\mathbf{d} - Hu_k)_i^2 \nu_k^u(du) + \int [H(u - u_k)]_i^2 \nu_k^u(du) \\ &= (\mathbf{d} - Hu_k)_i^2 + \mathbf{e}_i^T H \mathcal{C}_p H^* \mathbf{e}_i, \end{aligned} \quad (2.31)$$

where \mathbf{e}_i ($i = 1, \dots, N_d$) represents the vector with the i -th element being equal to 1 and all of the other elements being equal to 0, and Proposition 1.18 in (Prato, 2006) is employed to derive the second equality. It can be seen from (2.31) that the adjoint equations, forward equations, and inverse of the operator \mathcal{C}_p^{-1} are needed with N_d times of iterative calculations to update the parameters $\{\beta_i^k\}_{i=1}^{N_d}$. This is a time consuming procedure when N_d is large, which is one of the main reasons that only relatively easy i.i.d noises could be considered in the conventional VI framework (Jia et al., 2021c; Jin and Zou, 2010).

2.3 Variational inverting network

Let us provide some observations of the classical VI algorithm as follows:

- The prior probability measure needs to be specified manually, i.e., the mean function \bar{u}_0 and the covariance operator \mathcal{C}_0 are required to be pre-specified. This makes the usage of the algorithm highly rely on the subjective experiences of the practitioner.
- When the practitioner acquires some new data, the whole iterative procedure should be implemented from scratch to obtain a new estimate, which is time consuming for many applications.

Inspired by the recent work on denoising tasks under the FD setting (Yue et al., 2019, 2020), we introduce some parametric form of posterior probability measure by adopting deep neural networks. The goal is to resolve both of the above two issues of current VI algorithms. To illustrate the idea, we provide some analysis on the posterior probability measures given by (2.24) and (2.29).

It follows from the formula as shown in Example 6.23 of (Stuart, 2010) that the expression of the mean function (2.25) can be written into the following form:

$$\bar{u}_p = (H^* \Sigma_{\text{inv}}^* H + \mathcal{C}_0^{-1})^{-1} H^* \Sigma_{\text{inv}}^* \mathbf{d} + (H^* \Sigma_{\text{inv}}^* H + \mathcal{C}_0^{-1})^{-1} \mathcal{C}_0^{-1} \bar{u}_0. \quad (2.32)$$

Denote $\{e_j\}_{j=1}^\infty$ in (2.2) and let $\{\lambda_j\}_{j=1}^\infty$ be a positive sequence belonging to ℓ^2 . In addition, we assume that the forward operator H can be decomposed into $S \circ F$ (only needed in Theorem 5), where

$$(Fu)(x) = \sum_{j=1}^\infty \lambda_j \langle u, e_j \rangle e_j(x) = \sum_{j=1}^\infty \lambda_j u_j e_j(x) \quad \forall u \in \mathcal{H}_u \quad (2.33)$$

and

$$(S \circ F)u = ((Fu)(x_1), \dots, (Fu)(x_{N_d}))^T \quad \forall (x_1, \dots, x_{N_d}) \in \mathbb{R}^{N_d}. \quad (2.34)$$

Theorem 5 Assume that the forward operator H can be decomposed into $S \circ F$, where F and S are defined in (2.33) and (2.34), respectively. Then, we have

$$\lim_{\max_{1 \leq i \leq N_d} \beta_i^* \rightarrow 0} \|(H^* \Sigma_{\text{inv}}^* H + \mathcal{C}_0^{-1})^{-1} \mathcal{C}_0^{-1} \bar{u}_0\|_{\mathcal{H}_u} = 0, \quad (2.35)$$

where

$$\Sigma_{\text{inv}}^* = \text{diag} \left(\frac{\alpha_1^*}{\beta_1^*}, \dots, \frac{\alpha_{N_d}^*}{\beta_{N_d}^*} \right) \quad (2.36)$$

with α_i^*, β_i^* ($i = 1, \dots, N_d$) being positive real numbers.

The proof is given in Subsection 5.2 of Appendix. It can be seen from Theorem 5 that the posterior mean \bar{u}_p of the function parameter u is not related to the prior mean function \bar{u}_0 when the noises are vanishing. This observation indicates that it is appropriate to introduce a deep neural network, named DNet (denoising network), to learn the noise information from the training examples. The DNet takes noisy data as the input and delivers denoised data as the output. For the denoised data, the corresponding parameters $\{\beta_i^*\}_{i=1}^{N_d}$ are extremely small. However, the denoised data cannot match the clean data exactly, i.e., the second term in (2.32) will not be exactly zero. To encode the information provided by the prior mean function, we introduce another deep neural network, named ENet (enhancing network), which takes the input as the estimate provided by the first term in (2.32) and produces the output as the final estimate. DNet and ENet can be combined together to compose a new deep neural network named INet (inverting network), which takes noisy data as the input and makes the estimated mean function as the output. This intuitive illustration is only focused on the mean function and covariance operators are omitted for simplicity. To incorporate complete statistical information, we introduce the parametric form of posterior measures by some deep neural networks. Then, the information of the noises and the prior measure can be incorporated into the parameters introduced in the posterior probability measures through some training data-set.

Based on the above discussion, we introduce the following parametric form of posterior probability measures:

$$\nu^u = \mathcal{N}(\bar{u}_p(\mathbf{d}; W_I), \mathcal{C}_p(\mathbf{d}; W_I)), \quad \nu^\sigma = \prod_{i=1}^{N_d} \text{IG}(\alpha_i(\mathbf{d}; W_S), \beta_i(\mathbf{d}; W_S)), \quad (2.37)$$

where $\{\alpha_i(\mathbf{d}; W_S)\}_{i=1}^{N_d}$, $\{\beta_i(\mathbf{d}; W_S)\}_{i=1}^{N_d}$ are represented by neural networks with parameters denoted by W_S , $\{\bar{u}_p(\mathbf{d}; W_I), \mathcal{C}_p(\mathbf{d}; W_I)\}$ are represented by neural networks with parameters denoted by W_I ($\mathcal{C}_p(\mathbf{d}; W_I)$ is a symmetric, positive definite, and trace class operator). The neural networks with parameters W_S and W_I are called SNet (sigma network) and INet, respectively. The INet may include two small DNNs, e.g., DNet and ENet. The specific structures of the INet can be found in Subsection 3.1 when presenting numerical examples. However, the general inference framework constructed in this section has no such restrictions on the INet. To formulate an optimization problem for the network parameters of INet and SNet, we need to find out the variational lower bound under the ID setting, which requires the following basic assumption.

Assumption 6 *The approximate probability measure ν with components ν^u and ν^σ and the posterior probability measure $\mu^{\mathbf{d}}$ are assumed to be equivalent to the prior probability measure μ_0 .*

Regarding the logarithm of the marginal likelihood, we have

$$\begin{aligned} \log Z_{\mathbf{d}} &= \int_{\mathcal{H}_u \times (\mathbb{R}^+)^{N_d}} \log Z_{\mathbf{d}} \nu(du, d\sigma) \\ &= \int_{\mathcal{H}_u \times (\mathbb{R}^+)^{N_d}} \log \left\{ \frac{d\mu_0}{d\nu} \frac{d\nu}{d\mu^{\mathbf{d}}} \frac{1}{\sqrt{\det(\Sigma)}} \exp \left(-\frac{1}{2} \|\Sigma^{-1/2}(\mathbf{d} - Hu)\|^2 \right) \right\} \nu(du, d\sigma). \end{aligned}$$

Expanding the terms in the integrand of the above equality yields

$$\log Z_{\mathbf{d}} = \mathcal{L}(u, \boldsymbol{\sigma}; \mathbf{d}) + D_{\text{KL}}(\nu || \mu^{\mathbf{d}}), \quad (2.38)$$

where

$$\mathcal{L}(u, \boldsymbol{\sigma}; \mathbf{d}) = \int \log \frac{d\mu_0}{d\nu} - \frac{1}{2} \log(\det(\Sigma)) - \frac{1}{2} \|\Sigma^{-1/2}(\mathbf{d} - Hu)\|^2 \nu(du, d\boldsymbol{\sigma}). \quad (2.39)$$

Noting that the KL divergence between the variational approximate measure ν and the true posterior measure $\mu^{\mathbf{d}}$ is non-negative, we can thus get

$$\log Z_{\mathbf{d}} \geq \mathcal{L}(u, \boldsymbol{\sigma}; \mathbf{d}). \quad (2.40)$$

Since $\mathcal{L}(u, \boldsymbol{\sigma}; \mathbf{d})$ constitutes a lower bound of $\log Z_{\mathbf{d}}$, we call it evidence lower bound (ELBO) as in the FD setting (Bishop, 2006). Under Assumption 6, we know that the optimization problems

$$\min_{W_I, W_S} D_{\text{KL}}(\nu || \mu^{\mathbf{d}}) \quad (2.41)$$

and

$$\min_{W_I, W_D} -\mathcal{L}(u, \boldsymbol{\sigma}; \mathbf{d}) \quad (2.42)$$

are equivalent to each other. The ELBO can be decomposed into the following three terms:

$$\mathcal{L}(u, \boldsymbol{\sigma}; \mathbf{d}) = I_1 + I_2 + I_3, \quad (2.43)$$

where

$$I_1 = \int \frac{d\mu_0^u}{d\nu^u} \nu^u(du), \quad I_2 = \int \frac{d\mu_0^\sigma}{d\nu^\sigma} \nu^\sigma(d\boldsymbol{\sigma}), \quad (2.44)$$

$$I_3 = \int -\frac{1}{2} \log(\det(\Sigma)) - \frac{1}{2} \|\Sigma^{-1/2}(\mathbf{d} - Hu)\|^2 \nu(du, d\boldsymbol{\sigma}). \quad (2.45)$$

Term I_1 . Different from the FD case, we can hardly reduce the form of I_1 . However, for some specific problems, we can use the reparameterization trick to approximate it by the Monte Carlo (MC) estimation, i.e.,

$$I_1 \approx \frac{d\mu_0^u}{d\nu^u}(\tilde{u}), \quad (2.46)$$

where $\tilde{u} = \bar{u}_p(\mathbf{d}; W_I) + \mathcal{C}_p(\mathbf{d}; W_I)^{1/2} \eta$ with $\eta \sim \mathcal{N}(0, \text{Id})$.

Term I_2 . Since $\boldsymbol{\sigma}$ belongs to the FD space, we may follow (Yue et al., 2019) and obtain

$$\begin{aligned} \int \log \frac{d\nu^\sigma}{d\mu_0^\sigma} \nu^\sigma(d\boldsymbol{\sigma}) &= \sum_{i=1}^{N_d} \left\{ (\alpha_i - \alpha_i^0 + 1) \psi(\alpha_i) + \alpha_i \left(\frac{\beta_i^0}{\beta_i} - 1 \right) \right. \\ &\quad \left. + (\alpha_i^0 - 1) (\log \beta_i - \log \beta_i^0) + [\log \Gamma(\alpha_i^0 - 1) - \log \Gamma(\alpha_i)] \right\}, \end{aligned} \quad (2.47)$$

where $\Gamma(\cdot)$ and $\psi(\cdot)$ represent the Gamma and Degamma functions, respectively.

Term I_3 . For the first term in I_3 , we have

$$\begin{aligned} -\frac{1}{2} \int \log(\det(\Sigma)) \nu(du, d\sigma) &= -\frac{1}{2} \sum_{i=1}^{N_d} \int \log \sigma_i^2 \nu^\sigma(d\sigma) \\ &= -\frac{1}{2} \sum_{i=1}^{N_d} (\log \beta_i - \psi(\alpha_i)). \end{aligned} \quad (2.48)$$

For the second term in I_3 , a simple calculation yields

$$-\frac{1}{2} \int \|(\mathbf{d} - Hu)\|_{\Sigma}^2 \nu(du, d\sigma) = -\frac{1}{2} \int (\mathbf{d} - Hu)^T \Sigma_{\text{inv}} (\mathbf{d} - Hu) \nu^u(du), \quad (2.49)$$

where

$$\Sigma_{\text{inv}} = \text{diag} \left(\mathbb{E}^{\nu^\sigma} [\sigma_1^{-1}], \dots, \mathbb{E}^{\nu^\sigma} [\sigma_{N_d}^{-1}] \right) = \text{diag} \left(\frac{\alpha_1}{\beta_1}, \dots, \frac{\alpha_{N_d}}{\beta_{N_d}} \right). \quad (2.50)$$

Using (2.48)–(2.49) and the MC estimate, we get

$$I_3 \approx -\frac{1}{2} \sum_{i=1}^{N_d} (\log \beta_i - \psi(\alpha_i)) - \frac{1}{2} (\mathbf{d} - H\tilde{u})^T \Sigma_{\text{inv}} (\mathbf{d} - H\tilde{u}), \quad (2.51)$$

where $\tilde{u} = \bar{u}_p(\mathbf{d}; W_I) + \mathcal{C}_p(\mathbf{d}; W_I)^{1/2} \eta$ with $\eta \sim \mathcal{N}(0, \text{Id})$.

For a given training data set $\{\mathbf{d}_i, u_i\}_{i=1}^{N_e}$, where N_e is a positive integer, we can construct the following objective function (i.e., the negative ELBO on the entire training set) to optimize the network parameters of INet and SNet:

$$\min_{W_I, W_S} - \sum_{i=1}^{N_e} \mathcal{L}(u^{(i)}, \sigma^{(i)}; \mathbf{d}^{(i)}), \quad (2.52)$$

where $u^{(i)}$, $\sigma^{(i)}$, and $\mathbf{d}^{(i)}$ denote the corresponding variables for the i -th training pair.

In the end of this subsection, we present a preliminary analysis for the estimation error of the mean function, which tends to provide some intuitions for future study. The proof is given in Subsection 5.2 of Appendix.

Theorem 7 *Let u^\dagger be the background truth function, \bar{u}_p be the estimated function given by (2.32), and \mathbb{E}_0 be the expectation corresponding to the distribution of the data. Then the following estimate holds:*

$$\begin{aligned} \mathbb{E}_0[\|\bar{u}_p(\mathbf{d}; W_I) - u^\dagger\|_{\mathcal{H}_u}] &\leq \mathbb{E}_0[\|\bar{u}_p(\mathbf{d}; W_I) - \bar{u}_p\|_{\mathcal{H}_u}] + \|\bar{u}_0 - u^\dagger\|_{\mathcal{H}_u} \\ &\quad + \text{tr}(\mathcal{C}_p H^* \Sigma_{\text{inv}}^* \Sigma \Sigma_{\text{inv}}^* H \mathcal{C}_p^*)^{1/2}, \end{aligned} \quad (2.53)$$

where Σ is the background truth noise covariance matrix and Σ_{inv}^* is the diagonal matrix $\text{diag}(\alpha_1^*/\beta_1^*, \dots, \alpha_{N_d}^*/\beta_{N_d}^*)$ defined in (2.21).

It can be seen that the proposed parametric form of posterior probability measures is an approximation of the probability measure derived from the IDVI method, provided that the unknown synthetic truth is known under some average sense. We have the following observations on the three terms appearing in (2.53).

The first term on the right-hand side of (2.53) reflects the approximation error arising from learning by DNNs, which can be analyzed in details, e.g., by introducing the concepts of sample error and approximation error (Cucker and Smale, 2001). The DNNs employed here need to learn a nonlinear operator between two separable Hilbert spaces, which, to the best of our knowledge, can hardly be analyzed under the current learning theory. However, there are some work for the learnability of the nonlinear operators (Chen and Chen, 1995) that should be useful for future investigations.

The second term accounts for the error induced by the synthetic function parameter used for training and the true background function. This term can also hardly be analyzed under the current form since u^\dagger and \bar{u}_0 cannot be obtained in the inverse computational stage. However, we could assume that the residual of the synthetic function and the background truth can be bounded by some constant with high probability. The third term on the right-hand side of (2.53) represents the errors induced by noises and the prior covariance operator.

2.4 Parametric strategies

In the implementation of the algorithm, it is required to choose appropriate prior probability measure μ_0 and approximate probability measure ν to ensure Assumption 6. This subsection is concerned with a possible parametric strategy.

For the finite-dimensional parameter σ , there is no singular issues of the prior and posterior probability measures. Hence, we focus on the more problematic function parameter u . The major difficulty is that Gaussian measures defined on ID space are singular with each other when the covariance operators are scaled by different constants. It still remains to be an open question on how to resolve such a singularity problem in terms of theory and optimal algorithms (Agapiou et al., 2014; Dunlop et al., 2017).

First, let us introduce some assumptions (proposed in (Dashti and Stuart, 2017)) that help to define appropriate covariance operators in the prior and posterior probability measures.

Assumption 8 (Dashti and Stuart, 2017) *The operator A , densely defined on the Hilbert space $\mathcal{H} = L^2(\Omega; \mathbb{R})$ where $\Omega \subset \mathbb{R}^d$ is a bounded domain with smooth boundary, satisfies the following properties:*

1. *A is positive definite, self-adjoint and invertible;*
2. *The eigenfunctions $\{e_j\}_{j \in \mathbb{N}}$ of A form an orthonormal basis for \mathcal{H} ;*
3. *The eigenvalues of A satisfy $\lambda_j \asymp j^{2/d}$;*
4. *There is $C > 0$ such that*

$$\sup_{j \in \mathbb{N}} \left(\|e_j\|_{L^\infty} + \frac{1}{j^{1/d}} \text{Lip}(e_j) \right) \leq C,$$

where $Lip(e_j)$ denotes the Lipschitz constant of $e_j, j = 1, \dots, \infty$.

With Assumption 8, we now restrict the prior probability measure of u to be $\mu_0^u = \mathcal{N}(\bar{u}, \mathcal{C}_{\epsilon_0})$ with $\mathcal{C}_{\epsilon_0} = (\epsilon_0^{-1} \text{Id} + \delta A^{\alpha/2})^{-2}$. Here, the parameters $\epsilon_0, \delta > 0$ are positive constants satisfying $\delta \ll \epsilon_0^{-1}$, and the parameter $\alpha > d/2$ controls the regularity properties of the generated random samples. The mean function \bar{u} is taken as the simulated background truth which is available at the training stage and cannot be obtained at the inference stage.

Remark 9 *When solving inverse problems, we usually can hardly obtain absolutely correct background true parameters as training data set. For example, in the geophysical applications, the “Marmousi” model, as a typical synthetic model (Haber and Tenorio, 2003), is frequently employed for training. Hence, we may choose the simulated background truth as the prior mean function, and the covariance operator accounts for the uncertainty information due to the inaccuracy of the training data set.*

For the posterior probability measure $\nu^u = \mathcal{N}(\bar{u}_p(\mathbf{d}; W_I), \mathcal{C}_p(\mathbf{d}; W_I))$, we specify the covariance operator as follows:

$$\mathcal{C}_p(\mathbf{d}; W_I) = (a(\mathbf{d}; W_I) \text{Id} + \delta A^{\alpha/2})^{-2}, \quad (2.54)$$

where α and δ are taken the same as the prior measure, and $a(\mathbf{d}; W_I)$ is a positive function parameterized by the neural network with parameters W_I . In the following, we let $\mathcal{H}_u = \mathcal{H}$ which is defined in Assumption 8.

The following result illustrates that μ_0^u and ν^u defined above are equivalent under some general conditions.

Theorem 10 *Assume that $\Omega \subset \mathbb{R}^d$ ($d \leq 3$) is a bounded domain with smooth boundary, and the function $a(\mathbf{d}; W_I) \in L^\infty(\Omega)$ has positive lower and upper bounds, i.e., $0 < \underline{a} \leq a(\mathbf{d}; W_I)(x) \leq \bar{a}$ for all $x \in \Omega$ with $\underline{a}, \bar{a} \in \mathbb{R}^+$. Assume that the mean functions \bar{u} and $\bar{u}_p(\mathbf{d}; W_I)$ introduced in μ_0^u and ν^u belong to the Hilbert scale $\mathcal{C}_{\epsilon_0}^{1/2} \mathcal{H}_u$. Then, the approximate posterior measure ν^u is equivalent to the prior measure μ_0^u .*

The proof is given in Subsection 5.2 of Appendix.

3. Numerical Examples

In this section, we give the specific settings of INet and SNet for inverse problems of PDEs. Then, we apply the VINet to two examples. One is a simple smoothing model that is widely used for a benchmark test (Agapiou et al., 2014) and another is an inverse source problem of the Helmholtz equation.

3.1 Network structures

In Section 2, we introduce a general neural network parameterized IDVI framework, where any type of rational neural networks can be chosen. However, well-constructed neural networks usually perform better and need smaller training data set, which are crucial for practical applications.

The INet proposed in the general inference framework has three types of functionalities:

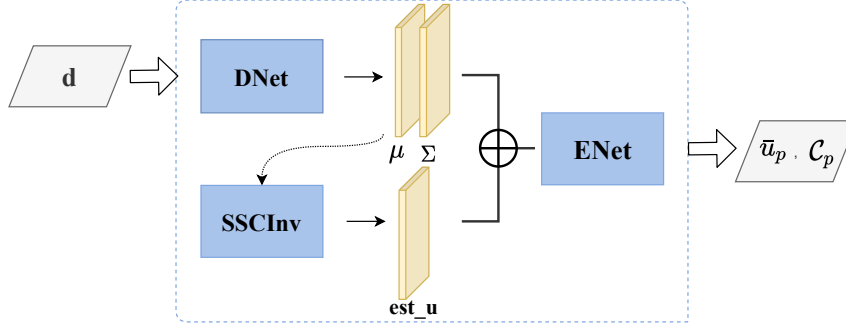


Figure 1: General structure of INet.

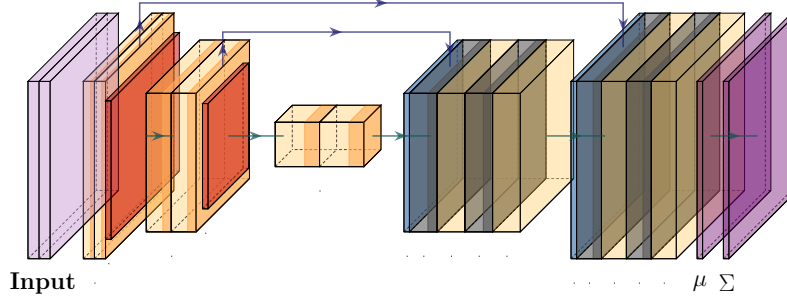


Figure 2: The tiny U-Net architecture employed for constructing DNet.

1. The network should be able to faithfully deliver the information of the noises ϵ , which is assumed to be distributed according to some non-i.i.d. Gaussian distribution.
2. The network is expected to have the ability to learn the prior information from the training data set, which can be utilized to provide high-quality estimations.
3. The forward evaluation of the network can be calculated efficiently compared with the classical iterative algorithm.

Based on the above three criteria, we design a specific INet structure, which is illustrated in Figure 1. The network contains three components. The first component, named as DNet, undertakes the denoising task, which is expected to learn the noise structure and provides estimated clean data. The second component, named as SSCInv, is chosen to be an extremely small scale classical inversion, in which every inverse of sparse matrices can be explicitly calculated and the results are some dense matrices. Clearly, only matrix multiplications are needed during the computations, which can be more efficiently implemented compared with solving linear equations. The third component, named as ENet, can be viewed as an enhancing layer, which learns the residual of the inexact inversion obtained by SSCInv layer with the background truth. More details of the three components are listed as follows:

1. DNet is chosen to be a small U-Net architecture as illustrated in Figure 2, which contains 3 encoder blocks, 2 decoder blocks and symmetric skip connection under each scale.

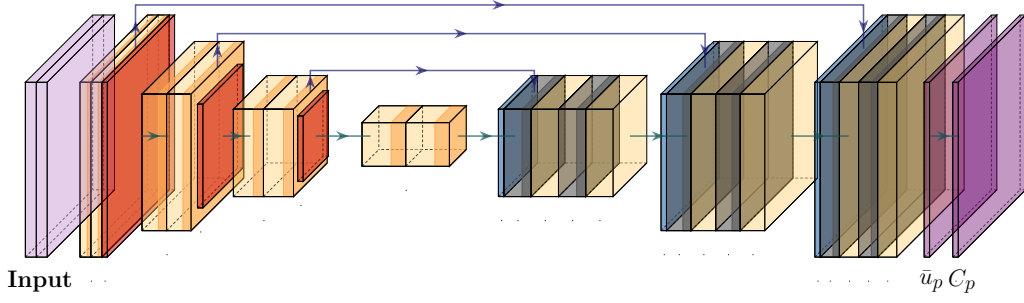


Figure 3: The U-Net architecture employed for constructing ENet.

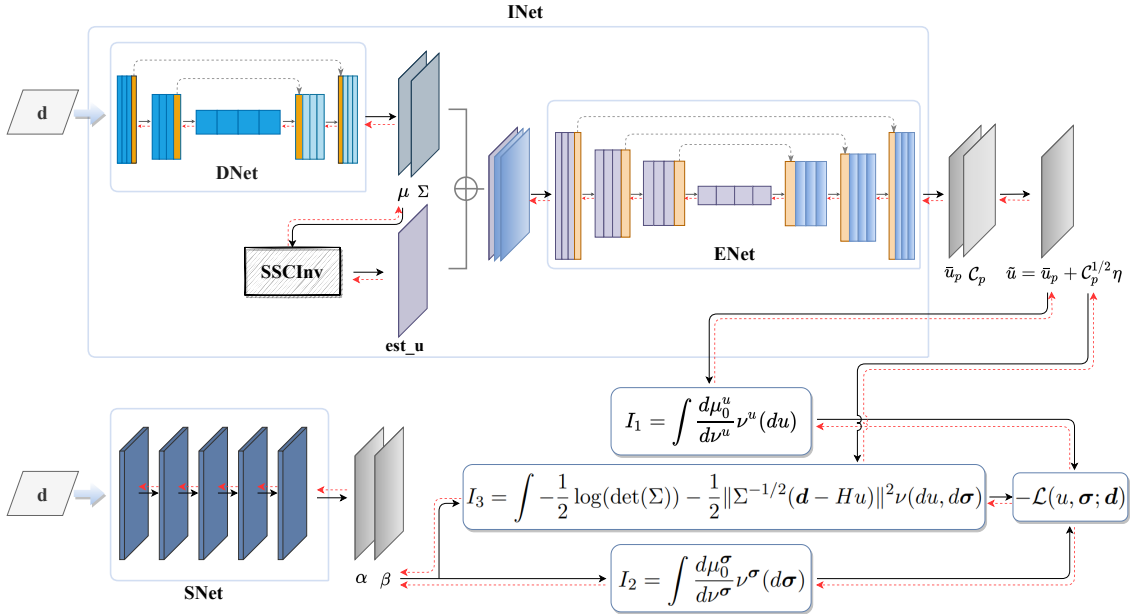


Figure 4: A particular example of the VINet framework.

2. An extremely small scale classical inversion (may be different for each problem) is employed as the SSCInv layer that provides a low resolution estimate (may contain some artifacts).
3. ENet is also chosen to be a U-Net as illustrated in Figure 3, which contains 4 encoder blocks, 3 decoder blocks and symmetric skip connection under each scale.

As for the SNet, it is adopted to infer the variational posterior parameters $\{\alpha_i(\mathbf{d}; W_S)\}_{i=1}^\infty, \{\beta_i(\mathbf{d}; W_S)\}_{i=1}^\infty$ from the noisy measurement data \mathbf{d} . Similar to the FD denoising case (Yue et al., 2019), we use the DnCNN (Zhang et al., 2017) architecture with five layers, and the feature channels of each layer is set to be 64.

Combining INet and SNet, we obtain the whole framework, which is illustrated in Figure 4. It is easy to train our model based on the objective function presented in (2.52) by using the stochastic gradient descent (SGD) algorithm or any variant optimization techniques. As for the FD case, each term of (2.43) can be intuitively explained. The terms I_1 and

I_2 control the discrepancy between the variational posteriors and the priors, mainly used to update INet and SNet, respectively. The term I_3 corresponds to the likelihood of the observed noisy data in the training data set, which couples INet and SNet together and generates gradients simultaneously during backpropagation.

For any new noisy data \mathbf{d} , through feeding it into the trained INet, the final estimated result can be directly obtained in an explicit manner. Additionally, by inputting the noisy data to SNet, the noise distribution information, even with complicated non-i.i.d. configurations, can be easily inferred.

Remark 11 *It should be mentioned that the ENet is a mapping between two ID spaces, which prefers to be specified as a neural network with dimension independent property. Recently, three types of neural networks with dimension independent properties (Bhattacharya et al., 2021; Nelsen and Stuart, 2021; Li et al., 2020) have been proposed to learn the non-linear mappings induced by PDEs. It is a hard problem to construct neural networks with dimension independent properties and the development is just in its initial stage. Since the focus of this work is to provide a general inference framework that is well-defined on infinite-dimensional space, we will not pursue this direction and just readily use classical U-Nets for simplicity.*

Numerically, the related PDEs are solved by using the finite element method, which is implemented by employing the open software FEniCS (Version 2019.1.0). The additional information on FEniCS can be found in (Logg et al., 2012). The related neural networks are implemented by employing the open software PyTorch (Version 1.7.0+cu110). For the mesh of the finite element method, it is generated automatically by FEniCS command `UnitSquareMesh(·)`. Since the mesh is regular, the finite difference discretization can also be adopted based on the same grid points. Hence, we used the finite difference method to generate the samples and compute the integral formulas involved in Terms 1 and 3 of the loss functional (2.43).

3.2 A simple smoothing model

3.2.1 BASIC SETTINGS

Consider an inverse source problem of the elliptic equation

$$\begin{aligned} -\alpha \Delta w + w &= u \quad \text{in } \Omega, \\ \frac{\partial w}{\partial \mathbf{n}} &= 0 \quad \text{on } \partial\Omega, \end{aligned} \tag{3.1}$$

where $\Omega = [0, 1]^2 \subset \mathbb{R}^2$, $\alpha > 0$ is a positive constant, and \mathbf{n} denotes the outward normal vector. The forward operator H is defined as follows:

$$Hu = (w(\mathbf{x}_1), w(\mathbf{x}_2), \dots, w(\mathbf{x}_{N_d}))^T, \tag{3.2}$$

where $u \in \mathcal{H}_u := L^2(\Omega)$, w denotes the solution of (3.1), and $\mathbf{x}_i \in \Omega$ for $i = 1, \dots, N_d$. In our implementations, the measurement points $\{\mathbf{x}_i\}_{i=1}^{N_d}$ are taken at the coordinates $\{(\frac{k}{20}, \frac{\ell}{20})\}_{k, \ell=1}^{20}$. To avoid the inverse crime (Kaipio and Somersalo, 2005), we discretize

the elliptic equation by the finite element method on a regular mesh (the grid points are uniformly distributed on the rectangular domain) with the number of grid points being equal to 300×300 . All of the training and testing data pairs are generated based on this discretization. In the inverse stage, the related functions are discretized by finite element method on a regular mesh with the number of grid points being equal to 128×128 .

For the operator A in Assumption 8 used in the prior probability measure, it is chosen to be the negative Laplace operator with Neumann boundary condition, which is similar to (Bui-Thanh et al., 2013). Hence, the operators in Subsection 2.4 can be specified explicitly as follows:

$$\mathcal{C}_{\epsilon_0} = (\epsilon_0^{-1} \text{Id} + \delta(-\Delta)^{\alpha/2})^{-2}, \quad \mathcal{C}_p(\mathbf{d}; W_I) = (a(\mathbf{d}; W_I) \text{Id} + \delta(-\Delta)^{\alpha/2})^{-2}.$$

To simplify the numerical implementations, we choose $\alpha = 2$ that makes the operators \mathcal{C}_{ϵ_0} and $\mathcal{C}_p(\mathbf{d}; W_I)$ to be discretized as illustrated in (Bui-Thanh et al., 2013). Since the fractional Laplace operator needs to be discretized differently (Bui-Thanh and Nguyen, 2016; Lischke et al., 2020), we leave the case $\alpha \neq 2$ to our future research.

Concerned with the SSInv layer, we employed a classical truncated singular value method (Engl et al., 1996). Specifically, the inverse method can be written in the form

$$R_{\lambda_m} \hat{\mathbf{d}} = q_{\lambda_m}(H^* H) H^* \hat{\mathbf{d}}, \quad (3.3)$$

where $\hat{\mathbf{d}}$ is the output of the DNet, and

$$q_{\lambda_m}(\lambda) = \begin{cases} \lambda^{-1}, & \lambda \geq \lambda_m \\ 0, & \lambda < \lambda_m. \end{cases} \quad (3.4)$$

Here, λ_m denotes a predefined truncate level. In the SSInv layer, the PDEs are discretized on a regular mesh with the number of grid points being equal to 50×50 , which is relatively small compared with the forward discretization. Based on such a small mesh, we obtain an inaccurate approximation with all of the related sparse matrices generated by the finite element method that can be inverted directly.

In our experiments, the training and testing function parameters u are generated by a Gaussian probability measure with mean zero and covariance given by

$$\mathcal{C}^{-1} = (\text{Id} - \nabla \cdot (\Theta \nabla \cdot))^2, \quad (3.5)$$

where $\Theta := \text{diag}(10, 1)$. Training and testing data sets contain 1000 and 100 randomly generated function parameters u with the measurements calculated by (3.1) under fine mesh. In Figure 5, three randomly generated functions are shown for the training and testing data.

Previous studies (Yue et al., 2019, 2020) imply that multiplicative noises can be removed efficiently by non-i.i.d. noise model. Hence, multiplicative noises are added on the clean data \mathbf{d}_c to generate noisy data \mathbf{d} in order to test the performance of the proposed VINet on non-i.i.d. noise cases. In the training stage, we add noises according to $\mathbf{d} = \mathbf{d}_c + a(\boldsymbol{\eta} \odot \mathbf{d}_c)$ where \odot is element-wise product, $\boldsymbol{\eta} \sim \mathcal{N}(0, \text{Id})$ and $a \sim U[-0.1, 0.1]$. In the testing stage, we take $a = 0.1$, i.e., $\mathbf{d} = \mathbf{d}_c + 0.1(\boldsymbol{\eta} \odot \mathbf{d}_c)$ where $\boldsymbol{\eta} \sim \mathcal{N}(0, \text{Id})$.

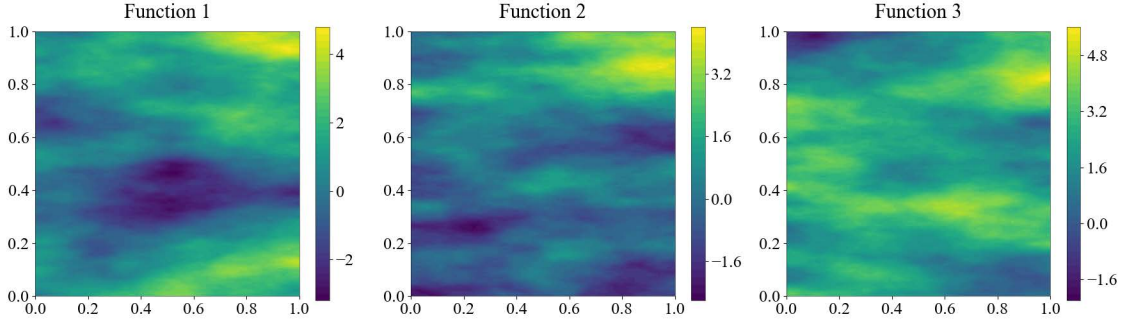


Figure 5: Three randomly generated functions u in training or testing data sets.

3.2.2 NUMERICAL RESULTS

We compare the results of VINet, mean-field based variational inference method (MFVI) exhibited in Algorithm 1, and truncated singular value decomposition (TSVD) method which is one of the most commonly adopted method dealing with ill-posed problems. For the MFVI method, the estimated function u highly depends on particular choices of the prior measure. Here, we assume that the distribution generating the truth is known, which means the statistical properties of the truth are known exactly for the MFVI method.

It is known that the MFVI method is computationally expensive. For calculating the mean function in the iteration, it is required to solve an adjoint PDE (corresponding to calculate H^*) and solve $2N_{ite}$ number of PDEs (corresponding to calculate \mathcal{C}_p) with N_{ite} being the maximum iteration number. For updating the parameter β , we need to calculate (2.31) which corresponds to $2N_d$ number (currently $N_d = 400$) of PDEs. In summary, we need to solve $2N_d + 2N_{ite} + 1$ (≥ 803 for the current case) number of PDEs during one iteration, which is not feasible for large- or even middle-scaled problems. Hence, for comparison purposes, we discretize PDEs on a regular 70×70 grid and compute the inverse of the sparse matrices that appear in the algorithm. Then, all of these expensive calculations can be computed in a reasonable time.

First, let us compare the estimates of the noise variances given by the MFVI and VINet. In Figure 6, we depict the estimated noise variances by the MFVI and VINet and the background true noise variances for three randomly selected testing examples. In the first line of Figure 6, the estimated variances of all 400 measurement points are given, which indicates that the VINet generates more accurate estimates than the MFVI (MFVI also provides reasonable estimates). In the second line of Figure 6, the estimated variances of only 100 measurement points are provided to give detailed comparisons. It is easy to note that the estimated variances given by the VINet are closer to the background truth than those obtained by the MFVI, which validates that the DNet and SNet can indeed learn the noise generating mechanism through training.

Next, let us compare the relative errors of the estimated functions obtained by the MFVI, TSVD, and VINet. The relative error is defined as follows:

$$\text{relative error} = \frac{\|\tilde{u} - u_{\text{truth}}\|_{L^2}}{\|u_{\text{truth}}\|_{L^2}}. \quad (3.6)$$

For the TSVD, different truncate levels lead to different estimates. To make full use of the TSVD, we take several different truncate levels as defined in (3.4), i.e., the truncate levels

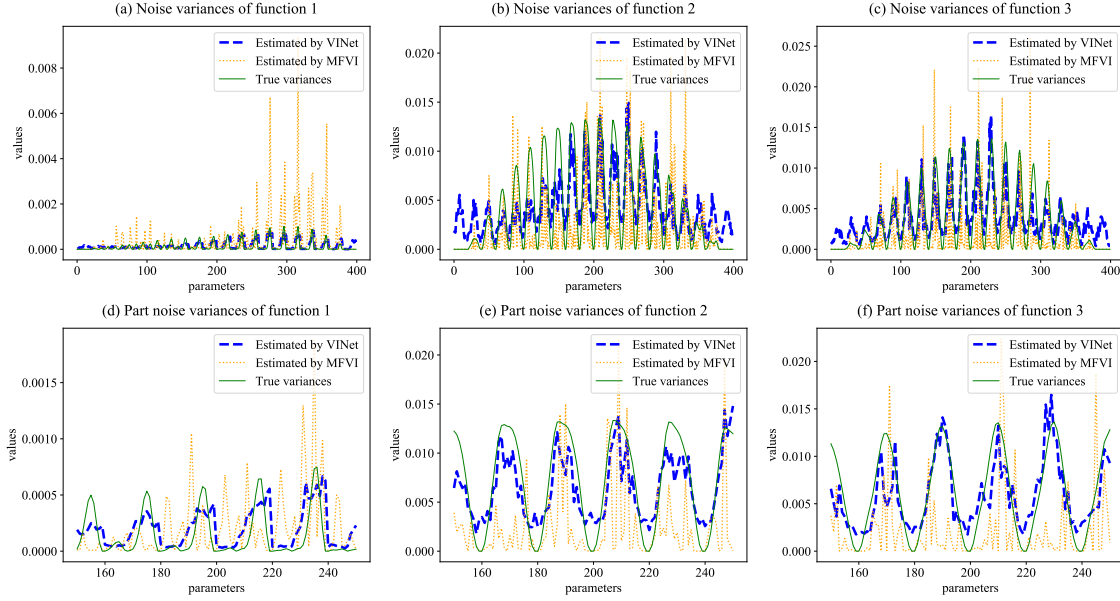


Figure 6: Comparison of the true and estimated noise variances by the MFVI and VINet.
 (a) (b) (c) Noise variances of all parameters for three different testing examples.
 (d) (e) (f) Partly enlarged illustration of (a), (b), and (c), respectively.

Table 1: Average relative errors of the estimates obtained by the TSVD.

Truncate Level	1	0.1	0.01	0.001	0.0001
Results with noisy data \mathbf{d}	0.5045	0.2911	0.6396	3.7324	4.4142
Results with clean data \mathbf{d}_c	0.5041	0.2761	0.1405	0.1214	0.1214

are set to be 1, 0.1, 0.01, 0.001, and 0.0001. Then we run the TSVD on 100 testing examples with noisy data \mathbf{d} and clean data \mathbf{d}_c , respectively. In Table 1, we show the relative errors obtained by the TSVD averaged on 100 testing examples when noisy data and clean data are employed. Due to numerical errors, we can see that the minimum average relative error obtained by the TSVD method is 0.1214 when clean data are employed. In practice, we can only use noisy data, which gives the minimum average relative error 0.2911 when the truncate level is 0.1.

Similarly, we also calculate the average relative errors for the estimates obtained by the MFVI and VINet. In Table 2, we present average relative errors for the estimates obtained by the MFVI, TSVD, and VINet with noisy and clean data, respectively. Obviously, in all cases, the proposed VINet provides the most accurate estimates. For the computing time, it seems that the TSVD takes the least amount of time. However, it should be emphasized that the computing time shown here for the TSVD excluded the computing time for performing singular value decomposition. In practice, it is hard to determine which truncate level

Table 2: Average relative errors of the estimates obtained by the TSVD.

	MFVI (noisy data)	TSVD (noisy data)	VINet (noisy data)
Average relative error	0.2530	0.2911	0.0681
	MFVI (clean data)	TSVD (clean data)	VINet (clean data)
Average relative error	0.2297	0.1214	0.0379
	MFVI	TSVD	VINet
Average computing time	44.3862 s	0.0038 s	0.0046 s

should be employed. Hence, there are several truncate levels that needs to be attempted, which inclines to make a further increase of its required computation time. For the VINet, we employed the same trained model for noisy data and clean data, i.e., no parameter tuning is needed in the inference stage. Another point that needs to be emphasized is that the computing time of the MFVI shown here is based on a small scale discretization (70×70 grid is employed, and all the procedures of solving PDEs are transformed into matrix multiplications) and 10 times of iteration. Actually, the computing time of the MFVI method for moderate or large-scale problems are extremely large. As a comparison, the VINet does not need to compute large-scale PDEs during the inference stage, and is thus efficient to conduct the inference.

At last, we show the background truth and estimates obtained by the MFVI, TSVD, and VINet when using noisy data for two testing examples in Figure 7. From sub-figures (b), (c), (f), and (g), we see that the MFVI and TSVD methods give unreasonable estimates which are possibly due to the large multiplicative noises and the strong smoothing property of the forward operator. The trained VINet can remove noises and enhance the estimates by the learned prior information. Although the details are still lost to a certain extent, the general structure of the background truth can be accurately recovered, which reflects that the trained VINet indeed learns structure information encoded in the learning examples.

3.3 An inverse source problem

In this subsection, we consider an inverse source problem for the Helmholtz equation with multi-frequency data which was studied in (Bao et al., 2015)¹. Specifically speaking, we

1. Deep learning based methods are employed for statistical inverse problems under the FD setting for CT image reconstruction, PET image reconstruction, and MRI reconstruction (Arridge et al., 2019). For these problems, the finite-dimensional formulation is widely employed. However, to the best of our knowledge, there seems little such types of work focused on multi-frequency inverse source problems governed by the Helmholtz equation (one of the typical and important mathematical models usually defined on ID space (Bao et al., 2015)). So we compare the performance of the proposed method with the classical recursive linearization method (RLM), which should be sufficient to reveal the mechanism and superiority of the proposed method.

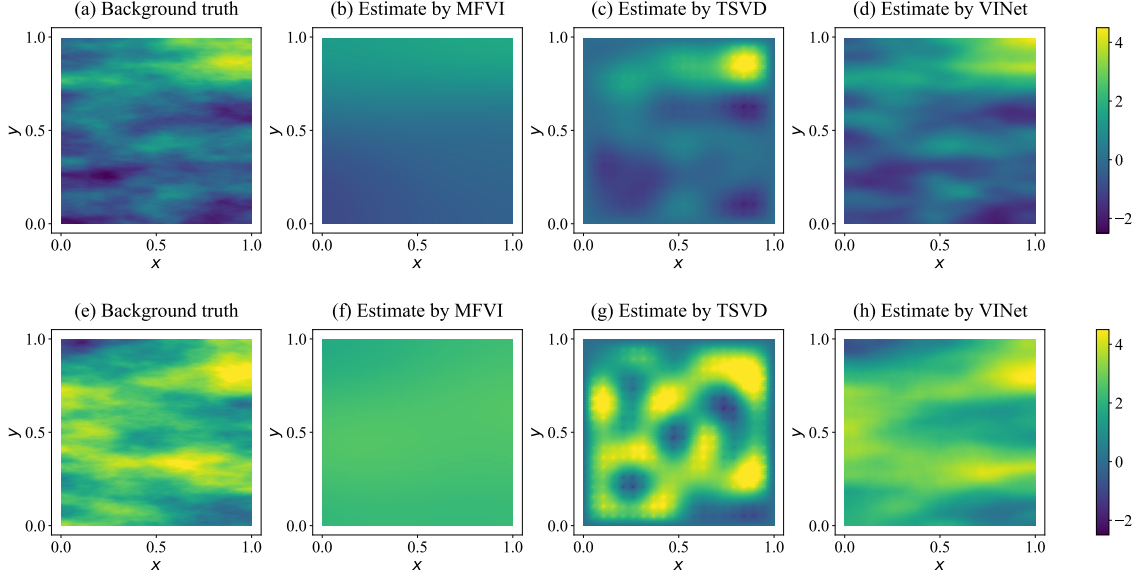


Figure 7: Comparison of the estimates obtained by the MFVI, TSVD, and VINet. (a) Background truth function 1; (b) Estimate given by the MFVI; (c) Estimate given by the TSVD with truncate level 0.1; (d) Estimate given by the VINet; (e) Background truth function 2; (f) Estimate given by the MFVI; (g) Estimate given by the TSVD with truncate level 0.1; (h) Estimate given by the VINet.

consider the following Helmholtz equation:

$$\begin{aligned} \Delta w + \kappa^2 w &= u \quad \text{in } \mathbb{R}^2, \\ \partial_r w - i\kappa w &= o(r^{-1/2}) \quad \text{as } r = |x| \rightarrow \infty, \end{aligned} \quad (3.7)$$

where κ is the wavenumber, w is the acoustic field, u is the acoustic source supported in an open bounded domain $\Omega = [0, 1]^2$. To simulate the problem defined on the infinity domain \mathbb{R}^2 , we adopt the perfectly matched layer (PML) technique and reformulate the scattering problem in a bounded domain. Denote $\mathbf{x} = (x, y) \in \mathbb{R}^2$. Let D be a rectangle containing Ω and let d_1 and d_2 be the thickness of the PML layers along the x and y directions, respectively. Denote by ∂D the boundary of the domain D . Let $s_1(x) = 1 + i\sigma_1(x)$ and $s_2(y) = 1 + i\sigma_2(y)$ be the model medium property, where σ_1, σ_2 are the positive continuous even functions and satisfy $\sigma_1(x) = 0, \sigma_2(y) = 0$ in Ω . Please refer to (Bao et al., 2010) for more details of the PML.

Following the general idea in designing PML absorbing layers, we may deduce the truncated PML problem:

$$\begin{aligned} \nabla \cdot (s \nabla w) + \kappa^2 s_1 s_2 w &= u \quad \text{in } D, \\ w &= 0 \quad \text{on } \partial D, \end{aligned} \quad (3.8)$$

where $s = \text{diag}(s_2(y)/s_1(x), s_1(x)/s_2(y))$ is a diagonal matrix. The forward operator related to κ is defined by the above Helmholtz equation $H_\kappa(u) = (w(\mathbf{x}_1), \dots, w(\mathbf{x}_{N_d}))^T$ with

$\{\mathbf{x}_i\}_{i=1}^{N_d} \in \partial\Omega$ and $u \in \mathcal{H}_u := L^2(\Omega)$. Since we consider the multi-frequency case, i.e., a series of wavenumbers $0 < \kappa_1 < \kappa_2 < \dots < \kappa_{N_f} < \infty$ are considered, the forward operator has the following form:

$$Hu = (H_{\kappa_1}(u), \dots, H_{\kappa_{N_f}}(u)) \in \mathbb{R}^{N_d \times N_{N_f}}. \quad (3.9)$$

Similar to the simple smoothing model, we generate the training and testing data based on a fine mesh with the number of grid points being equal to 500×500 . In the inverse computational stage, the related functions are discretized by the finite element method on a regular mesh with the number of grid points being equal to 160×160 . Concerned with the operators \mathcal{C}_{ϵ_0} and \mathcal{C}_p , we adopt exactly the same settings as those in Subsection 3.2 for the simple smoothing model.

For the SSCInv layer, we employ the classical RLM reviewed in (Bao et al., 2015) with $\kappa = 1, 2, \dots, 48$. The PDEs are discretized on a regular mesh with the number of grid points being equal to 40×40 , which makes it possible to directly compute the inverse of all the sparse matrices generated by the finite element method. Obviously, for a source function, the data generated by PDEs on a fine mesh with grid points being equal to 500×500 is different from the data obtained by PDEs on a coarse mesh, especially when the wavenumber is large. For this example, we take the data generated by PDEs on the fine mesh with random Gaussian noise as the noisy input data. To accelerate the convergence speed, we divide the training into two stages: the training process of DNet and SNet, and that of ENet and SNet. For the DNet training (stage 1 of training), we take the data calculated by PDEs on a coarse mesh as the accurate data, which makes the DNet learn the modeling error and random noise together. Please refer to (Calvetti et al., 2018; Jia et al., 2019) for some more relevant references on model error learning algorithms.

Before presenting the numerical results, we clarify how the training and testing datasets are constructed. Mimicking the strategies employed in (Jia et al., 2019), we introduce the following formula:

$$\tilde{u}(x, y) := \sum_{k=1}^3 (1-x^2)^{a_k^1} (1-y^2)^{a_k^2} a_k^3 \exp\left(-a_k^4(x-a_k^5)^2 - a_k^6(y-a_k^7)^2\right), \quad (3.10)$$

where

$$\begin{aligned} a_k^1, a_k^2 &\sim U[1, 3], & a_k^3 &\sim U[-1, 1], \\ a_k^4, a_k^6 &\sim U[8, 10], & a_k^5, a_k^7 &\sim U[-0.8, 0.8], \end{aligned}$$

with $k = 1, 2, 3$ and $U[a, b]$ is the uniform distribution between a and b . To demonstrate the effectiveness of the proposed method, we consider the following nonsmooth source function:

$$u(x, y) = \begin{cases} \tilde{u}(x, y) & \text{for } |\mathbf{x}| < r_1, \\ -0.5 & \text{for } r_2 \leq |\mathbf{x}| \leq r_1, \\ 0.0 & \text{for } |\mathbf{x}| > r_2, \end{cases} \quad (3.11)$$

where $r_1 \sim U[0.65, 0.75]$ and $r_2 \sim U[0.85, 0.95]$. Based on Eq. (3.11), we generate 1000 source functions for training and 100 source functions for testing, respectively. For testing

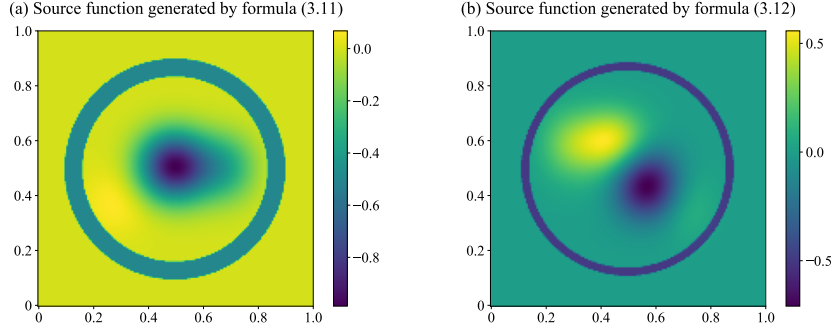


Figure 8: (a) One sample of the source function generated by formula (3.11); (b) One sample of the source function generated by formula (3.12).

the generalization properties, we also test the performance of the trained model on the following source function:

$$u^\dagger(x, y) = u(x, y) + \tilde{u}(x, y), \quad (3.12)$$

where u and \tilde{u} are two functions generated according to Eq. (3.11) and Eq. (3.10), respectively. The functions defined by (3.12) and (3.11) exhibit similar properties but the function defined in (3.12) can never be generated from Eq. (3.11), which mimics the following situation: the constructed learning examples usually cannot contain completely correct information, i.e., prior knowledge may exhibit bias. One thing that should be emphasized is that the training datasets can be constructed by employing more sophisticated methods and not restricted to the presented simple parametric form. To give the reader a visual illustration, we draw one of the samples generated by Eq. (3.11) and the source function generated by (3.12) in Figure 8.

In Figures 9 and 10, we show the results given by DNet with data generated by PDE solver discretized on a fine mesh and with added 5% random Gaussian noise when the source functions are chosen to be the functions shown in sub-figures (a) and (b) of Figure 8, respectively. Sub-figures (a) and (d) in Figures 9 and 10 depict that when the wavenumber is small, i.e., the data generated by the accurate and rough forward solvers have no large difference, the de-noised data and the noisy data cannot be distinguished visually compared with the clean data. However, as the wavenumber increases (wavelength decreases), the solutions of the accurate and rough forward solvers will demonstrate significant differences since finer mesh grid is needed to ensure that there are enough discrete grid points in one wavelength. From sub-figures (b), (c), (e), and (f) in Figures 9 and 10, it can be evidently seen that the rough forward solver cannot give similar measurements as the accurate forward solver, i.e., the rough forward solver may exhibit relatively large model error. When such crucial model error appears, data generated by the DNet are visually much similar to the clean data compared with the noisy data, which reflects that the DNet can learn the sophisticated model error mechanism between the accurate and rough forward solvers. Especially, the source function in sub-figure (b) of Figure 8 cannot be generated from Eq. (3.11), but the DNet can also finely compensate model errors when the wavenumber $\kappa = 25$. When the wavenumber $\kappa = 46$ (it is more difficult to compensate model errors for higher

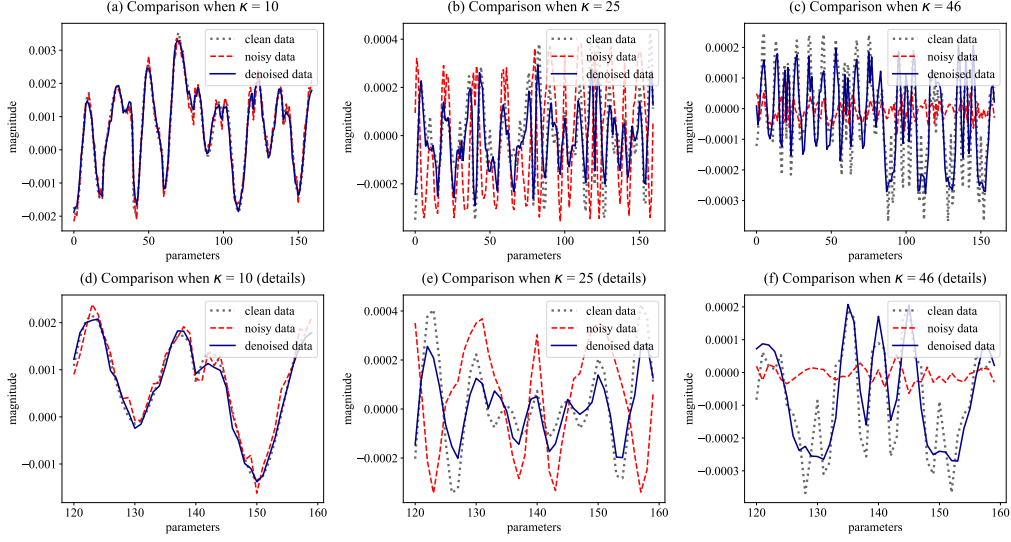


Figure 9: Noisy data (data generated by accurate forward solver with random Gaussian noise), clean data (data generated by rough forward solver), and denoised data (the output of the DNet) when taking the function shown in (a) of Figure 8 to be the source function u . (a) Data when the wavenumber $\kappa = 10$; (b) Data when the wavenumber $\kappa = 25$; (c) Data when the wavenumber $\kappa = 46$; (d)(e)(f) Partly enlarged versions of (a), (b), and (c), respectively.

wavenumbers), the DNet can also provide a reasonable result. These numerical results confirm the fine generalization capability of the proposed DNet.

Now, we compare the results obtained by the classical RLM (Bao et al., 2015) with the estimated mean functions obtained by the VINet. For the classical RLM, we employed two types of data, i.e., data \mathbf{d}_{48} obtained when the wavenumbers are $\kappa = 1, \dots, 48$ and data \mathbf{d}_{60} obtained when the wavenumbers are $\kappa = 1, 2, \dots, 60$. Recall that the proposed VINet used data \mathbf{d}_{48} . Figures 11 and 12 show the results when the background truth are specified as in sub-figures (a) and (b) of Figure 8, respectively. From the figures, it is obvious that the VINet can provide visually most reliable estimates compared with the classical RLM with \mathbf{d}_{48} and \mathbf{d}_{60} . The RLM with \mathbf{d}_{60} seems to provide more reasonable estimates than the RLM with \mathbf{d}_{48} since more data are employed. For providing more accurate estimates by using the RLM, we may need to use data generated by more wavenumbers. The background truth in Figure 12 is generated according to Eq. (3.12), which is different from the generating mechanism of the learning examples. In such a case, the VINet also provides a reasonable estimate, further validating that it possesses fine generalization property intrinsically.

Figures 11 and 12 only show one of the results among the 200 test examples generated according to Eq. (3.11) and Eq. (3.12) (100 test examples for each case). In Table 3, we provide quantitative comparisons on computing time and relative errors. From Table 3, it can be seen that the mean computing time of 100 test examples for the VINet are 0.449 and 0.439 seconds, evidently smaller than the mean computing time of the RLM. A much less computing time for the VINet can be expected since no forward PDEs is needed to be calculated during the inference stage. The relative errors for the VINet are much lower

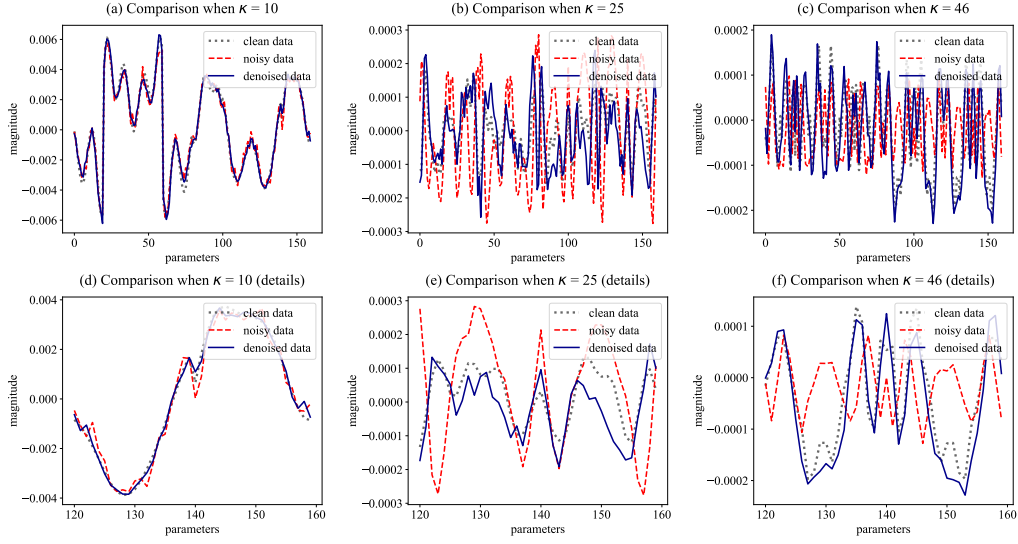


Figure 10: Noisy data (data generated by accurate forward solver with random Gaussian noise), clean data (data generated by rough forward solver), and denoised data (the output of the DNet) when taking the function shown in (b) of Figure 8 to be the source function u . (a) Data when the wavenumber $\kappa = 10$; (b) Data when the wavenumber $\kappa = 25$; (c) Data when the wavenumber $\kappa = 46$; (d)(e)(f) Partly enlarged versions of (a), (b), and (c), respectively.

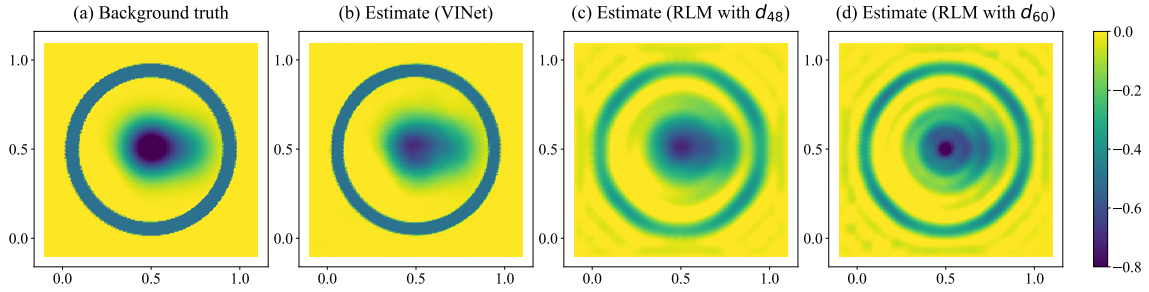


Figure 11: (a) Background true function generated according to Eq. (3.11); (b) Estimate obtained by the VINet with \mathbf{d}_{40} ; (c)(d) Estimates obtained by the RLM with \mathbf{d}_{40} and \mathbf{d}_{60} , respectively.

than that of the RLM with data \mathbf{d}_{48} and \mathbf{d}_{60} . This can be rationally explained by that the classical RLM only uses the information encoded in the data. However, the VINet encodes prior information into the network parameters efficiently through the learning process.

4. Conclusion

In this paper, we have studied inverse problems governed by PDEs with non-i.i.d. noise assumption under the Bayesian analysis framework. A rigorous illustration is provided for

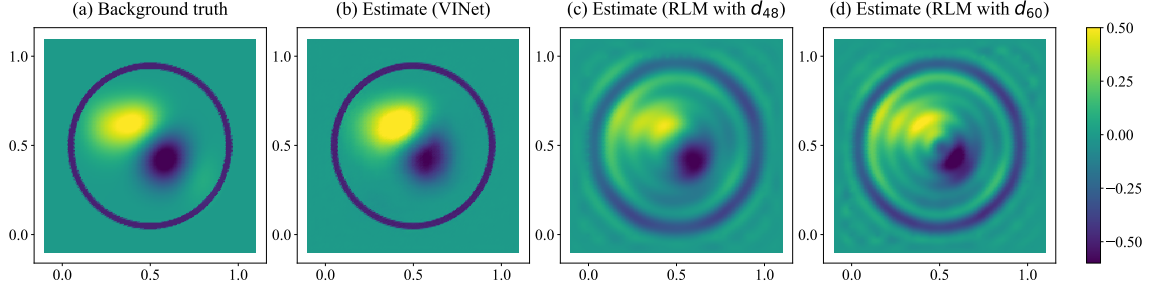


Figure 12: (a) Background true function generated according to Eq. (3.12); (b) Estimate obtained by the VINet with \mathbf{d}_{40} ; (c)(d) Estimates obtained by the RLM with \mathbf{d}_{40} and \mathbf{d}_{60} , respectively.

Table 3: Quantitative comparisons for the VINet (using data \mathbf{d}_{48}) and RLM (using data \mathbf{d}_{48} and \mathbf{d}_{60}).

Mean values based on 100 test examples generated from Eq. (3.11)		VINet	RLM (\mathbf{d}_{48})	RLM (\mathbf{d}_{60})
	Relative Error	0.014	0.295	0.258
	Computing Time	0.449 s	111.535 s	133.276 s
Mean values based on 100 test examples generated from Eq. (3.12)		VINet	RLM (\mathbf{d}_{48})	RLM (\mathbf{d}_{60})
	Relative Error	0.027	0.268	0.234
	Computing Time	0.439 s	110.407 s	132.957 s

the Bayes' formula under the non-i.i.d. noise setting with the conjugate prior measure. For constructing an efficient approximate sampling algorithm, we deduce the mean-field based variational inference (MFVI) method with infinite-dimensional parameters. However, the deduced algorithm is time-consuming since a large amount of computationally expensive PDEs need to be solved. To resolve this issue, we have further constructed a parametric form of posterior measures based on intuitive analysis of the approximate measure proposed in MFVI method and propose a general inference framework for inverse problems named VINet. By introducing measure equivalence conditions, the evidence lower bound (ELBO) argument has been generalized to the infinite-dimensional setting, which yields a computable training method. A possible parametric strategy of the parametric posterior measure is given, which reflects the equivalent measure assumption that can be satisfied by designing parametric strategies appropriately. Finally, we provide a possible specific network structure that yields a concrete VINet. The VINet has been applied to two inverse problems that are governed by a simple elliptic equation and the Helmholtz equation. For both inverse

problems, the VINet can learn prior information of interested function and noises from training examples efficiently and provide proper estimates quickly.

The current VINet framework is proposed based on the analysis on the MFVI method under the conjugate prior measure, which restricts the form of the posterior measures. Especially for nonlinear inverse problems, the VINet can only manage the linearized problems and provide an approximate probability measure. As for the MFVI, the approximate probability measure may be inaccurate for some highly nonlinear problems. Hence, generalizing the semi-conjugate VI methods to the infinite-dimensional setting and constructing the corresponding DNN-based inference method is worthy to be investigated in future work. For the current preliminary studies on numerical aspects, we only employ the classical U-Net, which is not designed for particular inverse problems. For specific inverse problems such as the inverse scattering problems, special neural networks (Khoo and Ying, 2019) may be employed to construct the INet in our general statistical inference framework. We will make further investigations on these issues in our future research.

5. Appendix

5.1 The infinite-dimensional variational inference theory

In this section, we provide a brief introduction to the infinite-dimensional variational inference theory without the mean-field assumption. For interested readers, we suggest reading the paper (Jia et al., 2021c) which comprehensively describes the full ideas and theories of this topic. It should be emphasized that we slightly ameliorate the statement of Theorem 11 in (Jia et al., 2021c) to make the theory more applicable to practical problems. See Theorem 13 below for details.

For inverse problems, it is required to find a probability measure μ^d on \mathcal{H} (some Hilbert space), which is called the posterior probability measure, specified by its density with respect to a prior probability measure μ_0 . Let the Bayesian formula on the Hilbert space be defined by

$$\frac{d\mu^d}{d\mu_0}(x) = \frac{1}{Z_{\mu^d}} \exp(-\Phi(x)), \quad (5.1)$$

where $\Phi(x) : \mathcal{H} \rightarrow \mathbb{R}$ is a continuous function, and $\exp(-\Phi(x))$ is integrable with respect to μ_0 . The constant Z_{μ^d} is chosen to ensure that μ^d is indeed a probability measure. The variational inference method can be formulated as solving the following optimization problem:

$$\arg \min_{\nu \in \mathcal{A}} D_{\text{KL}}(\nu || \mu), \quad (5.2)$$

where $\mathcal{A} \subset \mathcal{M}(\mathcal{H})$ is a set of measures. Here $\mathcal{M}(\mathcal{H})$ is the set of Borel probability measures on \mathcal{H} .

For a fixed positive constant M , we assume the variable $x = (x_1, \dots, x_M)$. Restricted to the settings in the main text, the constant $M = 2$ and $x = (u, \sigma)$. Generally, the Hilbert

space \mathcal{H} and set \mathcal{A} may be specified as

$$\mathcal{H} = \prod_{j=1}^M \mathcal{H}_j, \quad \mathcal{A} = \prod_{j=1}^M \mathcal{A}_j, \quad (5.3)$$

where $\mathcal{H}_j (j = 1, \dots, M)$ are a series of separable Hilbert spaces and $\mathcal{A}_j \subset \mathcal{M}(\mathcal{H}_j)$. Let $\nu := \prod_{i=1}^M \nu^i$ be a probability measure such that $\nu(dx) = \prod_{i=1}^M \nu^i(dx)$. With these assumptions, the minimization problem in (5.2) can be rewritten as

$$\arg \min_{\nu^i \in \mathcal{A}_i} D_{\text{KL}} \left(\prod_{i=1}^M \nu^i \parallel \mu^d \right) \quad (5.4)$$

for suitable sets \mathcal{A}_i with $i = 1, 2, \dots, M$. Now, we introduce the approximate probability measure ν given in (5.2) equivalent to μ_0 , defined by

$$\frac{d\nu}{d\mu_0}(x) = \frac{1}{Z_\nu} \exp(-\Phi_\nu(x)). \quad (5.5)$$

Compared with the finite-dimensional case, a natural way for introducing an independence assumption is to assume that the potential $\Phi_\nu(x)$ can be decomposed as

$$\exp(-\Phi_\nu(x)) = \prod_{j=1}^M \exp(-\Phi_\nu^j(x_j)), \quad (5.6)$$

where $x = (x_1, \dots, x_M)$. As illustrated in (Jia et al., 2021c), this intuitive idea prevents us from incorporating those parameters contained in the prior probability measure into the hierarchical Bayes' model. Given these considerations, the following assumption needs to be introduced.

Assumption 12 *Let us introduce a reference probability measure*

$$\mu_r(dx) = \prod_{j=1}^M \mu_r^j(dx_j), \quad (5.7)$$

which is equivalent to the prior probability measure with the following relation:

$$\frac{d\mu_0}{d\mu_r}(x) = \frac{1}{Z_0} \exp(-\Phi^0(x)). \quad (5.8)$$

For each $j = 1, 2, \dots, M$, there is a predefined continuous function $a_j(\epsilon, x_j)$ where ϵ is a positive number and $x_j \in \mathcal{H}_j$. Concerning these functions, we assume that $\mathbb{E}^{\mu_r^j}[a_j(\epsilon, \cdot)] < \infty$ where $\epsilon \in [0, \epsilon_0^j]$ with ϵ_0^j is a small positive number ($j = 1, \dots, M$). We also assume that the approximate probability measure ν is equivalent to the reference measure μ_r and that the Radon–Nikodym derivative of ν with respect to μ_r takes the following form

$$\frac{d\nu}{d\mu_r}(x) = \frac{1}{Z_r} \exp \left(- \sum_{j=1}^M \Phi_j^r(x_j) \right). \quad (5.9)$$

Following Assumption 12, we know that the approximate measure can be decomposed as $\nu(dx) = \prod_{j=1}^M \nu^j(dx_j)$ with

$$\frac{d\nu^j}{d\mu_r^j} = \frac{1}{Z_r^j} \exp(-\Phi_j^r(x_j)). \quad (5.10)$$

Here, $Z_r^j = \mathbb{E}^{\mu_r^j}(\exp(-\Phi_j^r(x_j)))$ ensures that ν^j is indeed a probability measure. For $j = 1, 2, \dots, M$, let \mathcal{Z}_j be defined as a Hilbert space that is embedded in \mathcal{H}_j . Then, for $j = 1, 2, \dots, M$, we introduce

$$\begin{aligned} R_j^1 &= \left\{ \Phi_j^r \mid \sup_{1/N \leq \|x_j\|_{\mathcal{Z}_j} \leq N} \Phi_j^r(x_j) < \infty \text{ for all } N > 0 \right\}, \\ R_j^2 &= \left\{ \Phi_j^r \mid \int_{\mathcal{H}_j} \exp(-\Phi_j^r(x_j)) \max(1, a_j(\epsilon, x_j)) \mu_r^j(dx_j) < \infty, \text{ for } \epsilon \in [0, \epsilon_0^j] \right\}, \end{aligned}$$

where ϵ_0^j and $a_j(\cdot, \cdot)$ are defined as in Assumption 12. With these preparations, we can define \mathcal{A}_j ($j = 1, 2, \dots, M$) as follows:

$$\mathcal{A}_j = \left\{ \nu^j \in \mathcal{M}(\mathcal{H}_j) \mid \begin{array}{l} \nu^j \text{ is equivalent to } \mu_r^j \text{ with (5.10) holding true,} \\ \text{and } \Phi_j^r \in R_j^1 \cap R_j^2 \end{array} \right\}. \quad (5.11)$$

Now, we state the main theorem that yield practical iterative algorithms.

Theorem 13 *Assume that the approximate probability measure in problem (5.4) satisfies Assumption 12. For $j = 1, 2, \dots, M$, we denote $T_N^j = \{x_j \mid 1/N \leq \|x_j\|_{\mathcal{Z}_j} \leq N\}$, with N being an arbitrary positive constant. For each reference measure μ_r^j , we assume that $\sup_N \mu_r^j(T_N^j) = 1$. In addition, we assume*

$$\sup_{x_i \in T_N^i} \int_{\prod_{j \neq i} \mathcal{H}_j} (\Phi^0(x) + \Phi(x)) 1_A(x) \prod_{j \neq i} \nu^j(dx_j) < \infty \quad (5.12)$$

and

$$\int_{\mathcal{H}_i} \exp\left(-\int_{\prod_{j \neq i} \mathcal{H}_j} (\Phi^0(x) + \Phi(x)) 1_{A^c}(x) \prod_{j \neq i} \nu^j(dx_j)\right) M_i(x) \mu_r^i(dx_i) < \infty, \quad (5.13)$$

where $A := \{x \mid \Phi^0(x) + \Phi(x) \geq 0\}$, and $M_i(x) := \max(1, a_i(\epsilon, x_i))$ with $i, j = 1, 2, \dots, M$. Then, problem (5.4) possesses a solution $\nu = \prod_{j=1}^M \nu^j \in \mathcal{M}(\mathcal{H})$ with the following form

$$\frac{d\nu}{d\mu_r} \propto \exp\left(-\sum_{i=1}^M \Phi_i^r(x_i)\right), \quad (5.14)$$

where

$$\Phi_i^r(x_i) = \int_{\prod_{j \neq i} \mathcal{H}_j} \left(\Phi^0(x) + \Phi(x)\right) \prod_{j \neq i} \nu^j(dx_j) + \text{Const} \quad (5.15)$$

and

$$\nu^i(dx_i) \propto \exp(-\Phi_i^r(x_i)) \mu_r^i(dx_i). \quad (5.16)$$

It should be pointed out that this theorem and the meanings of R_j^1 and R_j^2 ($j = 1, \dots, M$) are slightly different from the statements given in (Jia et al., 2021c). The proof of Theorem 11 in (Jia et al., 2021c) can be taken step by step to prove Theorem 13. Actually, the present version can be seen as a more appropriate amelioration of Theorem 11 in (Jia et al., 2021c), which can be verified more easily for practical problems.

5.2 Proof details

Proof of Theorem 2

Proof To prove the theorem, it suffices to verify the conditions given in Theorem 13. Specifically speaking, we need to verify the following four inequalities:

$$\begin{aligned} T_1 &= \sup_{u \in T_N^u} \int_{(\mathbb{R}^+)^{N_d}} \Phi(u, \boldsymbol{\sigma}) \nu^\sigma(d\boldsymbol{\sigma}) < \infty, \\ T_2 &= \sup_{\boldsymbol{\sigma} \in T_N^\sigma} \int_{\mathcal{H}_u} \Phi(u, \boldsymbol{\sigma}) \nu^\sigma \nu^u(du) < \infty, \\ T_3 &= \int_{(\mathbb{R}^+)^{N_d}} \exp\left(-\int_{\mathcal{H}_u} \Phi(u, \boldsymbol{\sigma}) \nu^u(du)\right) \max(1, a(\epsilon, \boldsymbol{\sigma})) \mu_0^\sigma(d\boldsymbol{\sigma}) < \infty, \\ T_4 &= \int_{\mathcal{H}_u} \exp\left(-\int_{(\mathbb{R}^+)^{N_d}} \Phi(u, \boldsymbol{\sigma}) \nu^\sigma(d\boldsymbol{\sigma})\right) \max(1, \|u\|_{\mathcal{H}_u}^2) \mu_0^u(du) < \infty. \end{aligned}$$

For term T_1 , we have

$$\begin{aligned} T_1 &\leq \sup_{u \in T_N^u} \frac{1}{2} \int_{(\mathbb{R}^+)^{N_d}} \left(\sum_{k=1}^{N_d} \frac{1}{\sigma_k} \|\mathbf{d} - Hu\|_2^2 + \sum_{k=1}^{N_d} \log \sigma_k \right) \nu^\sigma(d\boldsymbol{\sigma}) \\ &\leq \left(1 + \sup_{u \in T_N^u} \|\mathbf{d} - Hu\|_2^2 \right) \int_{(\mathbb{R}^+)^{N_d}} \sum_{k=1}^{N_d} \left(\frac{1}{\sigma_k} + \log \sigma_k \right) \nu^\sigma(d\boldsymbol{\sigma}) \\ &\leq C \int_{(\mathbb{R}^+)^{N_d}} \sum_{k=1}^{N_d} \left(\exp\left(\frac{\epsilon'}{\sigma_k}\right) + \sigma_k^{\epsilon'} \right) \nu^\sigma(d\boldsymbol{\sigma}) \\ &\leq C \int_{(\mathbb{R}^+)^{N_d}} \exp(-\Phi_\sigma(\boldsymbol{\sigma})) \max(1, a(2\epsilon', \boldsymbol{\sigma})) \mu_0^\sigma(d\boldsymbol{\sigma}) < \infty, \end{aligned}$$

where $\epsilon' < \epsilon_0/2$ and C is a generic constant that may be different from line to line.

For term T_2 , we have

$$T_2 \leq \sup_{\boldsymbol{\sigma} \in T_N^\sigma} \frac{1}{2} \sum_{k=1}^{N_d} \left(\frac{1}{\sigma_k} + \log \sigma_k \right) \int_{\mathcal{H}_u} (1 + \|\mathbf{d} - Hu\|_2^2) \nu^u(du).$$

Considering $\nu^u \in \mathcal{A}_u$, we get

$$\int_{\mathcal{H}_u} (1 + \|\mathbf{d} - Hu\|_2^2) \nu^u(du) \leq C \int_{\mathcal{H}_u} (1 + \|u\|_{\mathcal{H}_u}^2) \nu^u(du) < \infty$$

and

$$\sum_{k=1}^{N_d} \left(\frac{1}{\sigma_k} + \log \sigma_k \right) \leq \sum_{k=1}^{N_d} \left(\frac{1}{\sigma_k} + \sigma_k \right) \leq 2NN_d < \infty,$$

which indicates $T_2 < \infty$.

Using the estimate

$$\exp \left(- \int_{\mathcal{H}_u} \frac{1}{2} \left(\|d - Hu\|_{\Sigma}^2 + \sum_{k=1}^{N_d} \log \sigma_k \right) \nu^u(du) \right) \leq \exp \left(- \frac{1}{2} \sum_{k=1}^{N_d} \log \sigma_k \right),$$

we can estimate T_3 as follows:

$$\begin{aligned} T_3 &\leq \int_{(\mathbb{R}^+)^{N_d}} \prod_{k=1}^{N_d} \sigma_k^{-1/2} \max(1, a(\epsilon, \boldsymbol{\sigma})) \mu_0^{\boldsymbol{\sigma}}(d\boldsymbol{\sigma}) \\ &\leq \sqrt{N_d} \int_{(\mathbb{R}^+)^{N_d}} \sum_{k=1}^{N_d} \sigma_k^{-1/2} \max(1, a(\epsilon, \boldsymbol{\sigma})) \mu_0^{\boldsymbol{\sigma}}(d\boldsymbol{\sigma}) < \infty, \end{aligned}$$

where the last inequality follows from the properties of inverse Gamma distribution. Notice that

$$\begin{aligned} \exp \left(- \frac{1}{2} \int_{(\mathbb{R}^+)^{N_d}} \|d - Hu\|_2^2 + \sum_{k=1}^{N_d} \log \sigma_k \nu^{\boldsymbol{\sigma}}(d\boldsymbol{\sigma}) \right) \\ \leq \exp \left(- \frac{1}{2} \sum_{k=1}^{N_d} \int_{(\mathbb{R}^+)^{N_d}} \log \sigma_k \nu^{\boldsymbol{\sigma}}(\boldsymbol{\sigma}) \right) < \infty. \end{aligned}$$

Then, for term T_4 , we have

$$T_4 \leq C \int_{\mathcal{H}_u} \max(1, \|u\|_{\mathcal{H}_u}^2) \mu_0^u(du) < \infty. \quad (5.17)$$

The proof is completed by noting the general theory shown in Subsection 5.1 in the Appendix. ■

Proof of Theorem 5

Proof Let us firstly give the explicit form of the operator H^* . Taking $\mathbf{f} = (f_1, \dots, f_{N_d})^T \in \mathbb{R}^{N_d}$ and $g = \sum_{k=1}^{\infty} g_k e_k \in \mathcal{H}_u$, we have

$$\langle H^* \mathbf{f}, g \rangle_{L^2} = \langle \mathbf{f}, Hg \rangle_{\ell^2} = \sum_{k=1}^{\infty} \lambda_k g_k \langle \mathbf{f}, S e_k \rangle_{\ell^2} = \sum_{k=1}^{\infty} \lambda_k g_k \sum_{i=1}^{N_d} f_i e_k(x_i),$$

which implies

$$H^* \mathbf{f} = \sum_{k=1}^{\infty} \left(\sum_{i=1}^{N_d} f_i \lambda_k e_k(x_i) \right) e_k(x). \quad (5.18)$$

Then, we have

$$\begin{aligned}
 H^* \Sigma_{\text{inv}}^* H \bar{u}_0 &= \sum_{k=1}^{\infty} \lambda_k \bar{u}_{0k} H^* \Sigma_{\text{inv}}^* S e_k \\
 &= \sum_{k=1}^{\infty} \lambda_k \bar{u}_{0k} H^* (e_k(x_1) \alpha_1^* / \beta_1^*, \dots, e_k(x_{N_d}) \alpha_{N_d}^* / \beta_{N_d}^*)^T \\
 &= \sum_{j=1}^{\infty} \left(\sum_{i=1}^{N_d} \frac{\alpha_i^*}{\beta_i^*} \sum_{k=1}^{\infty} \lambda_k \bar{u}_{0k} e_k(x_i) \lambda_j e_j(x_i) \right) e_j(x).
 \end{aligned} \tag{5.19}$$

With these preparations, we find that

$$\begin{aligned}
 (H^* \Sigma_{\text{inv}}^* H + \mathcal{C}_0^{-1})^{-1} \mathcal{C}_0^{-1} \bar{u}_0 &= \\
 &= \sum_{j=1}^{\infty} \frac{\alpha_j^{-1}}{\sum_{i=1}^{N_d} \frac{\alpha_i^*}{\beta_i^*} \sum_{k=1}^{\infty} \lambda_k \frac{\bar{u}_{0k}}{\bar{u}_{0j}} e_k(x_i) \lambda_j e_j(x_i) + \alpha_j^{-1}} \bar{u}_{0j} e_j(x),
 \end{aligned} \tag{5.20}$$

which obviously implies the desired conclusion. \blacksquare

Proof of Theorem 7

Proof Based on Eq. (2.33), we have

$$\begin{aligned}
 \bar{u}_p &= \mathcal{C}_p \left[(H^* \Sigma_{\text{inv}}^* H + \mathcal{C}_0^{-1}) u^\dagger + H^* \Sigma_{\text{inv}}^* \epsilon + \mathcal{C}_0^{-1} (\bar{u}_0 - u^\dagger) \right] \\
 &= u^\dagger + \mathcal{C}_p \left[H^* \Sigma_{\text{inv}}^* \epsilon + \mathcal{C}_0^{-1} (\bar{u}_0 - u^\dagger) \right],
 \end{aligned} \tag{5.21}$$

which yields

$$\begin{aligned}
 \mathbb{E}_0 [\|\bar{u}_p - u^\dagger\|_{\mathcal{H}}] &\leq \mathbb{E}_0 [\|\mathcal{C}_p H^* \Sigma_{\text{inv}}^* \epsilon\|_{\mathcal{H}_u}] + \|\mathcal{C}_p \mathcal{C}_0^{-1} (\bar{u}_0 - u^\dagger)\|_{\mathcal{H}_u} \\
 &\leq \mathbb{E}_0 [\|\mathcal{C}_p H^* \Sigma_{\text{inv}}^* \epsilon\|_{\mathcal{H}_u}^2]^{1/2} + \|\bar{u}_0 - u^\dagger\|_{\mathcal{H}_u} \\
 &= \text{tr} (\mathcal{C}_p H^* \Sigma_{\text{inv}}^* \Sigma \Sigma_{\text{inv}}^* H \mathcal{C}_p^*)^{1/2} + \|\bar{u}_0 - u^\dagger\|_{\mathcal{H}_u}.
 \end{aligned} \tag{5.22}$$

Now, we have

$$\mathbb{E}_0 [\|\bar{u}_p(\mathbf{d}; W_I) - u^\dagger\|_{\mathcal{H}_u}] \leq \mathbb{E}_0 [\|\bar{u}_p(\mathbf{d}; W_I) - \bar{u}_p\|_{\mathcal{H}_u}] + \mathbb{E}_0 [\|\bar{u}_p - u^\dagger\|_{\mathcal{H}_u}], \tag{5.23}$$

which yields the required estimate by inserting the above inequality (5.22). \blacksquare

Proof of Theorem 10

Proof Because the operator A is assumed to be a self-adjoint and positive definite operator, it holds for appropriate f that

$$\langle (\underline{a} + \delta A^{\alpha/2}) f, f \rangle \leq \langle (a + \delta A^{\alpha/2}) f, f \rangle \leq \langle (\bar{a} + \delta A^{\alpha/2}) f, f \rangle, \tag{5.24}$$

where we denote $a := a(\mathbf{d}; W_I)$ and omit all of the identity operators. For conciseness, we omit the identity operators in the proof when there are no ambiguities from the context. Obviously, we also have

$$\langle (\underline{a} + \delta A^{\alpha/2})^2 f, f \rangle \leq \langle (a + \delta A^{\alpha/2})^2 f, f \rangle \leq \langle (\bar{a} + \delta A^{\alpha/2})^2 f, f \rangle, \quad (5.25)$$

when choosing appropriate f in each estimate. According to Theorem 2.25 (Feldman-Hajek theorem) in (Prato and Zabczyk, 2014), we only need to prove the following two results:

1. $\mathcal{C}_{\epsilon_0}^{1/2} \mathcal{H} = \mathcal{C}_p^{1/2} \mathcal{H} = \mathcal{H}_0$,
2. the operator $T := (\mathcal{C}_p^{-1/2} \mathcal{C}_{\epsilon_0}^{1/2})(\mathcal{C}_p^{-1/2} \mathcal{C}_{\epsilon_0}^{1/2})^* - \text{Id}$ is a Hilbert-Schmidt operator on $\bar{\mathcal{H}}_0$.

First, we prove (1). Taking arbitrary $u \in \mathcal{C}_{\epsilon_0}^{1/2} \mathcal{H}$ gives

$$u = \mathcal{C}_{\epsilon_0}^{1/2} v \quad \text{for some } v \in \mathcal{H}. \quad (5.26)$$

The variable can be rewritten as $u = \mathcal{C}_p^{1/2} \mathcal{C}_p^{-1/2} \mathcal{C}_{\epsilon_0}^{1/2} v$. Considering (5.25), we have

$$\begin{aligned} \|\mathcal{C}_p^{-1/2} \mathcal{C}_{\epsilon_0}^{1/2} v\|_{\mathcal{H}}^2 &= \|(a + \delta A^{\alpha/2})(\epsilon_0^{-1} + \delta A^{\alpha/2})^{-1} v\|_{\mathcal{H}}^2 \\ &\leq \|(\bar{a} + \delta A^{\alpha/2})(\epsilon_0^{-1} + \delta A^{\alpha/2})^{-1} v\|_{\mathcal{H}}^2 \\ &= \sum_{k=1}^{\infty} \left(\frac{\bar{a} + \delta \lambda_k^{\alpha/2}}{\epsilon_0^{-1} + \delta \lambda_k^{\alpha/2}} \right)^2 v_k^2 \\ &\leq C \|v\|_{\mathcal{H}}^2 < \infty, \end{aligned} \quad (5.27)$$

which implies $u \in \mathcal{C}_p^{1/2} \mathcal{H}$. Conversely, we assume $u \in \mathcal{C}_p^{1/2} \mathcal{H}$ with $u = \mathcal{C}_p^{1/2} v$ for some $v \in \mathcal{H}$. Similarly, we can rewrite $u = \mathcal{C}_{\epsilon_0}^{1/2} \mathcal{C}_{\epsilon_0}^{-1/2} \mathcal{C}_p^{1/2} v$. In the following, we give estimates of $\mathcal{C}_{\epsilon_0}^{-1/2} \mathcal{C}_p^{1/2} v$ which is more complex than the estimate (5.27). Obviously, we have

$$\|\mathcal{C}_{\epsilon_0}^{-1/2} \mathcal{C}_p^{1/2} v\|_{\mathcal{H}}^2 = \sum_{k,\ell=1}^{\infty} v_k v_{\ell} \langle \mathcal{C}_{\epsilon_0}^{-1/2} \mathcal{C}_p^{1/2} e_k, \mathcal{C}_{\epsilon_0}^{-1/2} \mathcal{C}_p^{1/2} e_{\ell} \rangle_{\mathcal{H}} = \sum_{k,\ell=1}^{\infty} v_k v_{\ell} B_{k,\ell}. \quad (5.28)$$

For the term $B_{k,\ell}$, we have

$$\begin{aligned} B_{k,\ell} &= \langle (a - \epsilon_0^{-1}) \mathcal{C}_p^{1/2} e_k, (a - \epsilon_0^{-1}) \mathcal{C}_p^{1/2} e_{\ell} \rangle_{\mathcal{H}} + 2 \langle (\epsilon_0^{-1} - a) \mathcal{C}_p^{1/2} e_k, e_{\ell} \rangle + \langle e_k, e_{\ell} \rangle \\ &= B_{k,\ell}^1 + B_{k,\ell}^2 + B_{k,\ell}^3. \end{aligned} \quad (5.29)$$

For the term $B_{k,\ell}^1$, we have

$$\begin{aligned} B_{k,\ell}^1 &\leq C \|(a + \delta A^{\alpha/2})^{-1} e_k\|_{\mathcal{H}} \|(a + \delta A^{\alpha/2})^{-1} e_{\ell}\|_{\mathcal{H}} \\ &\leq C \|(\underline{a} + \delta A^{\alpha/2})^{-1} e_k\|_{\mathcal{H}} \|(\underline{a} + \delta A^{\alpha/2})^{-1} e_{\ell}\|_{\mathcal{H}} \\ &= C \frac{1}{\underline{a} + \delta \lambda_k^{\alpha/2}} \frac{1}{\underline{a} + \delta \lambda_{\ell}^{\alpha/2}}. \end{aligned} \quad (5.30)$$

Hence, we further obtain

$$\sum_{k,\ell=1}^{\infty} B_{k,\ell}^1 \leq C \left[\sum_{k=1}^{\infty} \left(v_k^2 + \left(\frac{1}{\underline{a} + \delta \lambda_k^{\alpha/2}} \right)^2 \right) \right]^2 < \infty. \quad (5.31)$$

For the term $B_{k,\ell}^2$, we have the following estimate

$$\begin{aligned} \sum_{k,\ell=1}^{\infty} v_k v_{\ell} B_{k,\ell}^2 &= 2 \sum_k v_k \langle (\epsilon_0^{-1} - a) \mathcal{C}_p^{1/2} e_k, \sum_{\ell=1}^{\infty} v_{\ell} e_{\ell} \rangle_{\mathcal{H}} \\ &\leq C \sum_{k=1}^{\infty} \left(v_k^2 + \left(\frac{1}{\underline{a} + \delta \lambda_k^{\alpha/2}} \right)^2 \right) \|v\|_{\mathcal{H}} < \infty. \end{aligned} \quad (5.32)$$

For the term $B_{k,\ell}^3$, we find

$$\sum_{k,\ell=1}^{\infty} v_k v_{\ell} B_{k,\ell}^3 \leq \|v\|_{\mathcal{H}}^2 < \infty. \quad (5.33)$$

Inserting estimates from (5.31) to (5.33) into (5.28), we arrive at

$$\|\mathcal{C}_{\epsilon_0}^{-1/2} \mathcal{C}_p^{1/2} v\|_{\mathcal{H}}^2 < \infty. \quad (5.34)$$

Hence, the proof of (1) is completed. Before going further, we denote $\langle \cdot, \cdot \rangle_{\mathcal{H}_0} := \langle \cdot, \cdot \rangle_{\mathcal{C}_{\epsilon_0}^{1/2} \mathcal{H}} = \langle (\epsilon_0 + \delta A^{\alpha/2}) \cdot, (\epsilon_0 + \delta A^{\alpha/2}) \cdot \rangle_{\mathcal{H}}$. For proving (2), we introduce $\tilde{e}_j = \frac{1}{\epsilon_0^{-1} + \delta \lambda_j^{\alpha/2}} e_j$ for $j = 1, 2, \dots$, which is an orthonormal basis on $\mathcal{C}_{\epsilon_0}^{1/2} \mathcal{H}$. Following simple calculations, we obtain

$$\begin{aligned} \sum_{j=1}^{\infty} \langle T \tilde{e}_j, T \tilde{e}_j \rangle_{\mathcal{H}_0} &= \sum_{j=1}^{\infty} \langle (\mathcal{C}_p^{-1/2} \mathcal{C}_{\epsilon_0} \mathcal{C}_p^{-1/2} - \text{Id}) \tilde{e}_j, (\mathcal{C}_p^{-1/2} \mathcal{C}_{\epsilon_0} \mathcal{C}_p^{-1/2} - \text{Id}) \tilde{e}_j \rangle_{\mathcal{H}_0} \\ &= \sum_{j=1}^{\infty} (I_j^1 + I_j^2 + I_j^3), \end{aligned} \quad (5.35)$$

where

$$I_j^1 = \langle (\mathcal{C}_p^{-1/2} \mathcal{C}_{\epsilon_0} \mathcal{C}_p^{-1/2} - \mathcal{C}_{\epsilon_0}^{1/2} \mathcal{C}_p^{-1/2}) \tilde{e}_j, (\mathcal{C}_p^{-1/2} \mathcal{C}_{\epsilon_0} \mathcal{C}_p^{-1/2} - \mathcal{C}_{\epsilon_0}^{1/2} \mathcal{C}_p^{-1/2}) \tilde{e}_j \rangle_{\mathcal{H}_0},$$

$$I_j^2 = 2 \langle (\mathcal{C}_p^{-1/2} \mathcal{C}_{\epsilon_0} \mathcal{C}_p^{-1/2} - \mathcal{C}_{\epsilon_0}^{1/2} \mathcal{C}_p^{-1/2}) \tilde{e}_j, (\mathcal{C}_{\epsilon_0}^{1/2} \mathcal{C}_p^{-1/2} - \text{Id}) \tilde{e}_j \rangle_{\mathcal{H}_0},$$

$$I_j^3 = \langle (\mathcal{C}_{\epsilon_0}^{1/2} \mathcal{C}_p^{-1/2} - \text{Id}) \tilde{e}_j, (\mathcal{C}_{\epsilon_0}^{1/2} \mathcal{C}_p^{-1/2} - \text{Id}) \tilde{e}_j \rangle_{\mathcal{H}_0}.$$

Since I_j^2 can be bounded by I_j^1 combined with I_j^3 , we only focus on the estimates of I_j^1 and I_j^3 in the following.

Estimate of I_j^1 : Because

$$\begin{aligned} \mathcal{C}_p^{-1/2} \mathcal{C}_{\epsilon_0}^{1/2} - \text{Id} &= (a + \delta A^{\alpha/2})(\epsilon_0^{-1} + \delta A^{\alpha/2})^{-1} - \text{Id} \\ &= \left(a + \delta A^{\alpha/2} - \epsilon_0^{-1} - \delta A^{\alpha/2} \right) (\epsilon_0^{-1} + \delta A^{\alpha/2})^{-1} \\ &= (a - \epsilon_0^{-1})(\epsilon_0^{-1} + \delta A^{\alpha/2})^{-1}, \end{aligned} \quad (5.36)$$

we have

$$\begin{aligned} I_j^1 &= \langle (\mathcal{C}_p^{-1/2} \mathcal{C}_{\epsilon_0}^{1/2} - \text{Id}) \mathcal{C}_{\epsilon_0}^{1/2} \mathcal{C}_p^{-1/2} \tilde{e}_j, (\mathcal{C}_p^{-1/2} \mathcal{C}_{\epsilon_0}^{1/2} - \text{Id}) \mathcal{C}_{\epsilon_0}^{1/2} \mathcal{C}_p^{-1/2} \tilde{e}_j \rangle_{\mathcal{H}_0} \\ &= \langle (a - \epsilon_0^{-1}) B \tilde{e}_j, (a - \epsilon_0^{-1}) B \tilde{e}_j \rangle_{\mathcal{H}_0} \\ &= \langle \mathcal{C}_{\epsilon_0}^{-1/2} [(a - \epsilon_0^{-1}) B \tilde{e}_j], \mathcal{C}_{\epsilon_0}^{-1/2} [(a - \epsilon_0^{-1}) B \tilde{e}_j] \rangle_{\mathcal{H}} \\ &\leq 2I_j^{11} + 2I_j^{12}, \end{aligned} \quad (5.37)$$

where $B \tilde{e}_j := \mathcal{C}_{\epsilon_0} \mathcal{C}_p^{-1/2} \tilde{e}_j$ and

$$\begin{aligned} I_j^{11} &= \langle (\epsilon_0^{-1} + \delta A^{\alpha/2}) [a B \tilde{e}_j], (\epsilon_0^{-1} + \delta A^{\alpha/2}) [a B \tilde{e}_j] \rangle_{\mathcal{H}}, \\ I_j^{12} &= \epsilon_0^{-2} \langle (\epsilon_0^{-1} + \delta A^{\alpha/2}) B \tilde{e}_j, (\epsilon_0^{-1} + \delta A^{\alpha/2}) B \tilde{e}_j \rangle_{\mathcal{H}}. \end{aligned}$$

For the term I_j^{11} , we have

$$\begin{aligned} I_j^{11} &= \langle (\epsilon_0^{-1} + \delta A^{\alpha/2}) \sum_{k=1}^{\infty} \langle a B \tilde{e}_j, e_k \rangle_{\mathcal{H}} e_k, (\epsilon_0^{-1} + \delta A^{\alpha/2}) \sum_{\ell=1}^{\infty} \langle a B \tilde{e}_j, e_{\ell} \rangle_{\mathcal{H}} e_{\ell} \rangle_{\mathcal{H}} \\ &= \sum_{k=1}^{\infty} \langle a B \tilde{e}_j, e_k \rangle_{\mathcal{H}}^2 \left(\frac{1}{\epsilon_0^{-1} + \delta \lambda_k^{\alpha/2}} \right)^2 \\ &= \left(\frac{1}{\epsilon_0^{-1} + \delta \lambda_j^{\alpha/2}} \right)^2 \sum_{k=1}^{\infty} \left(\frac{1}{\epsilon_0^{-1} + \delta \lambda_k^{\alpha/2}} \right)^2 \langle e_j, \mathcal{C}_p^{-1/2} \mathcal{C}_{\epsilon_0} (a e_k) \rangle_{\mathcal{H}}^2. \end{aligned} \quad (5.38)$$

Because

$$\begin{aligned} &\sum_{j=1}^{\infty} \left(\frac{1}{\epsilon_0^{-1} + \delta \lambda_j^{\alpha/2}} \right)^2 \langle e_j, (a + \delta A^{\alpha/2})(\epsilon_0^{-1} + \delta A^{\alpha/2})^{-2} (a e_k) \rangle_{\mathcal{H}}^2 \\ &\leq C \|a e_k\|_{\mathcal{H}}^2 \sum_{j=1}^{\infty} \left(\frac{1}{\epsilon_0^{-1} + \delta \lambda_j^{\alpha/2}} \right)^2 < \infty, \end{aligned} \quad (5.39)$$

we obtain

$$\sum_{j=1}^{\infty} I_j^{11} \leq C \|a e_k\|_{\mathcal{H}}^2 \sum_{j=1}^{\infty} \left(\frac{1}{\epsilon_0^{-1} + \delta \lambda_j^{\alpha/2}} \right)^2 \sum_{k=1}^{\infty} \left(\frac{1}{\epsilon_0^{-1} + \delta \lambda_k^{\alpha/2}} \right)^2 < \infty. \quad (5.40)$$

For the term I_j^{12} , we have

$$\begin{aligned} I_j^{12} &= \langle (\epsilon_0^{-1} + \delta A^{\alpha/2})^{-1} (a + \delta A^{\alpha/2}) \tilde{e}_j, (\epsilon_0^{-1} + \delta A^{\alpha/2})^{-1} (a + \delta A^{\alpha/2}) \tilde{e}_j \rangle_{\mathcal{H}} \\ &\leq 2 \langle (\epsilon_0^{-1} + \delta A^{\alpha/2})^{-1} (a \tilde{e}_j), (\epsilon_0^{-1} + \delta A^{\alpha/2})^{-1} (a \tilde{e}_j) \rangle_{\mathcal{H}} \\ &\quad + 2 \delta^2 \langle (\epsilon_0^{-1} + \delta A^{\alpha/2})^{-1} A^{\alpha/2} \tilde{e}_j, (\epsilon_0^{-1} + \delta A^{\alpha/2})^{-1} A^{\alpha/2} \tilde{e}_j \rangle_{\mathcal{H}}. \end{aligned} \quad (5.41)$$

For the first term on the right-hand side of the above inequality, we have

$$\begin{aligned}
 & \langle (\epsilon_0^{-1} + \delta A^{\alpha/2})^{-1}(a\tilde{e}_j), (\epsilon_0^{-1} + \delta A^{\alpha/2})^{-1}(a\tilde{e}_j) \rangle_{\mathcal{H}} \\
 &= \langle (\epsilon_0^{-1} + \delta A^{\alpha/2})^{-1} \sum_{k=1}^{\infty} \langle a\tilde{e}_j, e_k \rangle e_k, (\epsilon_0^{-1} + \delta A^{\alpha/2})^{-1} \sum_{\ell=1}^{\infty} \langle a\tilde{e}_j, e_{\ell} \rangle e_{\ell} \rangle_{\mathcal{H}} \\
 &= \sum_{k=1}^{\infty} \langle a\tilde{e}_j, e_k \rangle_{\mathcal{H}}^2 \left(\frac{1}{\epsilon_0^{-1} + \delta \lambda_k^{\alpha/2}} \right)^2 \\
 &\leq \bar{a}^2 \left(\frac{1}{\epsilon_0^{-1} + \delta \lambda_j^{\alpha/2}} \right)^2 \sum_{k=1}^{\infty} \left(\frac{1}{\epsilon_0^{-1} + \delta \lambda_k^{\alpha/2}} \right)^2.
 \end{aligned} \tag{5.42}$$

For the second term on the right-hand side of (5.41), we have

$$\langle (\epsilon_0^{-1} + \delta A^{\alpha/2})^{-1} A^{\alpha/2} \tilde{e}_j, (\epsilon_0^{-1} + \delta A^{\alpha/2})^{-1} A^{\alpha/2} \tilde{e}_j \rangle_{\mathcal{H}} \leq C \left(\frac{1}{\epsilon_0^{-1} + \delta \lambda_j^{\alpha/2}} \right)^2. \tag{5.43}$$

Inserting estimates (5.42) and (5.43) into (5.41), we obtain

$$\sum_{j=1}^{\infty} I_j^{12} \leq C \sum_{j=1}^{\infty} \left(\frac{1}{\epsilon_0^{-1} + \delta \lambda_j^{\alpha/2}} \right)^2 < \infty. \tag{5.44}$$

Combining estimates (5.37), (5.40), and (5.44), we finally obtain

$$\sum_{j=1}^{\infty} I_j^1 < \infty. \tag{5.45}$$

Estimate of I_j^3 : For the term I_j^3 , we find that

$$\begin{aligned}
 I_j^3 &= \langle (\epsilon_0^{-1} + \delta A^{\alpha/2})^{-1}[(a - \epsilon_0^{-1})\tilde{e}_j], (\epsilon_0^{-1} + \delta A^{\alpha/2})^{-1}[(a - \epsilon_0^{-1})\tilde{e}_j] \rangle_{\mathcal{H}_0} \\
 &= \langle (a - \epsilon_0^{-1})\tilde{e}_j, (a - \epsilon_0^{-1})\tilde{e}_j \rangle_{\mathcal{H}} \\
 &\leq C \left(\frac{1}{\epsilon_0^{-1} + \delta \lambda_j^{\alpha/2}} \right)^2,
 \end{aligned} \tag{5.46}$$

which implies

$$\sum_{j=1}^{\infty} I_j^3 < \infty. \tag{5.47}$$

Combining estimates of I_j^1 and I_j^3 , we finally obtain

$$\sum_{j=1}^{\infty} \langle T\tilde{e}_j, T\tilde{e}_j \rangle_{\mathcal{H}_0} < \infty, \tag{5.48}$$

which indicates that T is a Hilbert–Schmidt operator. Hence, the proof is completed. \blacksquare

Acknowledgments

The first author was supported by the NSFC (Grant Nos. 11871392, 12090020, and 12090021). The third author was supported in part by the NSF grant DMS-1912704. The fourth author was supported by the NSFC (Grant Nos. 11690011 and U1811461) and the Macao Science and Technology Development Fund grant No. 061/2020/A2.

References

- J. Adler and O. Öktem. Deep Bayesian inversion. arXiv:1811.05910, 2018.
- S. Agapiou, S. Larsson, and A. M. Stuart. Posterior contraction rates for the Bayesian approach to linear ill-posed inverse problems. *Stoch. Proc. Appl.*, 123(10):3828–3860, 2013.
- S. Agapiou, J. M. Bardsley, O. Papaspiliopoulos, and A. M. Stuart. Analysis of the Gibbs sampler for hierarchical inverse problems. *SIAM/ASA J. Uncertainty Quantification*, 2: 511–544, 2014.
- S. Agapiou, O. Papaspiliopoulos, D. Sanz-Alonso, and A. M. Stuart. Importance sampling: intrinsic dimension and computational cost. *Stat. Sci.*, 32(3):405–431, 2017.
- S. Arridge, P. Maass, O. Öktem, and C.-B. Schönlieb. Solving inverse problems using data-driven models. *Acta Numer.*, 28:1–174, 2019.
- G. Bao, S. N. Chow, P. Li, and H. Zhou. Numerical solution of an inverse medium scattering problem with a stochastic source. *Inverse Probl.*, 26(7):074014, 2010.
- G. Bao, P. Li, J. Lin, and F. Triki. Inverse scattering problems with multi-frequencies. *Inverse Probl.*, 31(9):093001, 2015.
- J. O. Berger. *Statistical Decision Theory and Bayesian Analysis*. Springer, New York, second edition, 1980.
- A. Beskos, A. Jasra, E. A. Muzaffer, and A. M. Stuart. Sequential Monte Carlo methods for Bayesian elliptic inverse problems. *Stat. Comput.*, 25:727–737, 2015.
- K. Bhattacharya, B. Hosseini, N. B. Kovachki, and A. M. Stuart. Model reduction and neural networks for parametric PDEs. *SMAI Journal of Computational Mathematics*, 7: 121–157, 2021.
- Christopher M. Bishop. *Pattern Recognition and Machine Learning*. Springer, New York, 2006.
- T. Bui-Thanh and Q. P. Nguyen. FEM-based discretization-invariant MCMC methods for PDE-constrained Bayesian inverse problems. *Inverse Probl. Imag.*, 10(4):943–975, 2016.
- T. Bui-Thanh, O. Ghattas, J. Martin, and G. Stadler. A computational framework for infinite-dimensional Bayesian inverse problems part I: The linearized case, with application to global seismic inversion. *SIAM J. Sci. Comput.*, 35(6):A2494–A2523, 2013.

- D. Calvetti, M. M. Dunlop, E. Somersalo, and A. M. Stuart. Iterative updating of model error for Bayesian inversion. *Inverse Probl.*, 34(2):025008, 2018.
- T. Chen and H. Chen. Universal approximation to nonlinear operators by neural networks with arbitrary activation functions and its application to dynamical systems. *IEEE T. Neural. Network*, 6(4):904–917, 1995.
- S. L. Cotter, M. Dashti, J. C. Robinson, and A. M. Stuart. Bayesian inverse problems for functions and applications to fluid mechanics. *Inverse Probl.*, 25(11):115008, 2009.
- S. L. Cotter, G. O. Roberts, A. M. Stuart, and D. White. MCMC methods for functions: modifying old algorithms to make them faster. *Stat. Sci.*, 28(3):424–446, 2013.
- F. Cucker and S. Smale. On the mathematical foundations of learning. *B. Am. Math. Soc.*, 39(1):1–49, 2001.
- T. Cui, K. J. H. Law, and Y. M. Marzouk. Dimension-independent likelihood-informed MCMC. *J. Comput. Phys.*, 304:109–137, 2016.
- M. Dashti and A. M. Stuart. The Bayesian approach to inverse problems. *Handbook of Uncertainty Quantification*, pages 311–428, 2017.
- Masoumeh Dashti, Stephen Harris, and Andrew Stuart. Besov priors for Bayesian inverse problems. *Inverse Probl. Imag.*, 6(2):183–200, 2012.
- M. M. Dunlop, M. A. Iglesias, and A. M. Stuart. Hierarchical Bayesian level set inversion. *Stat. Comput.*, 27:1555–1584, 2017.
- M. M. Dunlop, D. Slepčev, A. M. Stuart, and M. Thorpe. Large data and zero noise limits of graph-based semi-supervised learning algorithms. *Appl. Comput. Harmon. A.*, 49(2): 655–697, 2020.
- H. W. Engl, M. Hanke, and A. Neubauer. *Regularization of Inverse Problems*. Kluwer Academic Publishers, Netherlands, 1996.
- L. C. Evans. *Partial Differential Equations*. American Mathematical Society, Providence, RI, second edition, 2010.
- Z. Feng and J. Li. An adaptive independence sampler MCMC algorithm for Bayesian inferences of functions. *SIAM J. Sci. Comput.*, 40(3):A1310–A1321, 2018.
- S. Ghosal and A. v. d. Vaart. *Fundamentals of Nonparametric Bayesian Inference*. Cambridge University Press, United States of America, 2017.
- M. Giordano and R. Nickl. Consistency of Bayesian inference with Gaussian process priors in an elliptic inverse problem. *Inverse Probl.*, 36(8):085001, 2020.
- E. Haber and L. Tenorio. Learning regularization functionals—a supervised training approach. *Inverse Probl.*, 19(3):611–626, 2003.

- F. Hoffmann, B. Hosseini, Z. Ren, and A. M. Stuart. Consistency of semi-supervised learning algorithms on graphs: probit and one-hot methods. *J. Mach. Learn. Res.*, 21(186):1–55, 2020.
- Bamdad Hosseini and Nilima Nigam. Well-posed Bayesian inverse problems: Priors with exponential tails. *SIAM/ASA J. Uncertainty Quantification*, 5(1):436–465, 2017.
- J. Jia, J. Peng, and J. Gao. Bayesian approach to inverse problems for functions with a variable index Besov prior. *Inverse Probl.*, 32(8):085006, 2016.
- J. Jia, S. Yue, J. Peng, and J. Gao. Infinite-dimensional Bayesian approach for inverse scattering problems of a fractional Helmholtz equation. *J. Funct. Anal.*, 275(9):2299–2332, 2018.
- J. Jia, B. Wu, J. Peng, and J. Gao. Recursive linearization method for inverse medium scattering problems with complex mixture Gaussian error learning. *Inverse Probl.*, 35(7):075003, 2019.
- J. Jia, P. Li, and D. Meng. Stein variational gradient descent on infinite-dimensional space and applications to statistical inverse problems. *arXiv:2102.09741*, 2021a.
- J. Jia, J. Peng, and J. Gao. Posterior contraction for empirical Bayesian approach to inverse problems under non-diagonal assumption. *Inverse Probl. Imag.*, 15(2):201–228, 2021b.
- J. Jia, Q. Zhao, Z. Xu, D. Meng, and Y. Leung. Variational Bayes’ method for functions with applications to some inverse problems. *SIAM J. Sci. Comput.*, 43(1):A355–A383, 2021c.
- B. Jin and J. Zou. Hierarchical Bayesian inference for ill-posed problems via variational method. *J. Comput. Phys.*, 229(19):7317–7343, 2010.
- J. Kaipio and E. Somersalo. *Statistical and Computational Inverse Problems*. Springer-Verlag, New York, 2005.
- H. Kekkonen, M. Lassas, and S. Siltanen. Posterior consistency and convergence rates for Bayesian inversion with hypoelliptic operators. *Inverse Probl.*, 32(8):085005, 2016.
- Y. Khoo and L. Ying. Switchnet: a neural network model for forward and inverse scattering problems. *SIAM J. Sci. Comput.*, (5):A3182–A3201, 2019.
- D. P. Kingma. Variational inference & deep learning: a new synthesis, 2017.
- B. T. Knapik, A. van Der Vaart, and J. H. van Zanten. Bayesian inverse problems with Gaussian priors. *Ann. Statist.*, 39:2626–2657, 2011.
- N. B. Kovachki and A. M. Stuart. Ensemble Kalman inversion: A derivative-free technique for machine learning tasks. *Inverse probl.*, 35(9):095005, 2019.
- M. Lassas and S. Siltanen. Can one use total variation prior for edge-preserving Bayesian inversion? *Inverse Probl.*, 20(5):1537, 2004.

- Matti Lassas, Eero Saksman, and Samuli Siltanen. Discretization-invariant Bayesian inversion and besov space priors. *Inverse Probl. Imag.*, 3, 2009.
- J. Latz. On the well-posedness of Bayesian inverse problems. *SIAM/ASA J. Uncertainty Quantification*, 8(1):451–482, 2020.
- Z. Li, N. Kovachki, K. Azizzadenesheli, B. Liu, K. Bhattacharya, A. M. Stuart, and A. Anandkumar. Neural operator: graph kernel network for partial differential equations. arXiv:2003.03485, 2020.
- A. Lischke, G. Pang, M. Gulian, F. Song, C. Glusa, X. Zheng, Z. Mao, W. Cai, M. M. Meerschaert, M. Ainsworth, and G. E. Karniadakis. What is the fractional Laplacian? A comparative review with new results. *J. Comput. Phys.*, 404(1):109009, 2020.
- A Logg, K. A. Mardal, and G. N. Wells. *Automated Solution of Differential Equations by the Finite Element Method*. Springer, 2012.
- N. H. Nelsen and A. M. Stuart. The random feature model for input-output maps between Banach spaces. arXiv:2005.10224, 2021.
- N. Petra, J. Martin, G. Stadler, and O. Ghattas. A computational framework for infinite-dimensional Bayesian inverse problems, part II: Stochastic Newton MCMC with application to ice sheet flow inverse problems. *SIAM J. Sci. Comput.*, 36(4):A1525–A1555, 2014.
- F. J. Pinski, G. Simpson, A. M. Stuart, and H. Weber. Kullback-Leibler approximation for probability measures on infinite dimensional space. *SIAM J. Math. Anal.*, 47(6):4091–4122, 2015a.
- F. J. Pinski, G. Simpson, A. M. Stuart, and H. Weber. Algorithms for Kullback-Leibler approximation of probability measures in infinite dimensions. *SIAM J. Sci. Comput.*, 37(6):A2733–A2757, 2015b.
- G. D. Prato. *An Introduction to Infinite-Dimensional Analysis*. Springer-Verlag, Berlin Heidelberg, 2006.
- G. D. Prato and J. Zabczyk. *Stochastic Equations in Infinite Dimensions*. Cambridge University Press, Cambridge, second edition, 2014.
- A. M. Stuart. Inverse problems: A Bayesian perspective. *Acta Numer.*, 19:451–559, 2010.
- S. Sun, G. Zhang, J. Shi, and R. Grosse. Functional variational Bayesian neural networks. In *ICLR*, 2019.
- B. Szabó, A. W. van der Vaart, and J. H. van Zanten. Frequentist coverage of adaptive nonparametric Bayesian credible sets. *Ann. Statist.*, 43(4):1391–1428, 2015.
- N. G. Trillos, Z. Kaplan, T. Samakhoana, and D. Sanz-Alonso. On the consistency of graph-based Bayesian semi-supervised learning and the scalability of sampling algorithms. *J. Mach. Learn. Res.*, 21(28):1–47, 2020.

- Sebastian J. Vollmer. Posterior consistency for Bayesian inverse problems through stability and regression results. *Inverse Probl.*, 29(12):125011, 2013.
- K. Wang, T. Bui-Thanh, and O. Ghattas. A randomized maximum a posteriori method for posterior sampling of high dimensional nonlinear Bayesian inverse problems. *SIAM J. Sci. Comput.*, 40(1):A142–A171, 2018.
- Z. Wang, T. Ren, J. Zhu, and B. Zhang. Function space particle optimization for Bayesian neural networks. In *ICLR*, 2019.
- J. Yoo, A. Wahab, and J. C. Ye. A mathematical framework for deep learning in elastic source imaging. *SIAM J. Appl. Math.*, 78(5):2791–2818, 2018.
- Z. Yue, H. Yong, Q. Zhao, L. Zhang, and D. Meng. Variational denoising network: toward blind noise modeling and removal. In *NeurIPS*, 2019.
- Z. Yue, H. Yong, Q. Zhao, L. Zhang, and D. Meng. Variational image restoration network. *ArXiv*, 2008.10796, 2020.
- C. Zhang, J. Butepage, H. Kjellstrom, and S. Mandt. Advances in variational inference. *IEEE T. Pattern Anal.*, 41(8):2008–2026, 2018.
- K. Zhang, W. Zuo, Y. Chen, D. Meng, and L. Zhang. Beyond a Gaussian denoiser: residual learning of deep CNN for image denoising. *IEEE T. Image Process.*, 26(7):3142–3155, 2017.
- Q. Zhou, T. Yu, X. Zhang, and J. Li. Bayesian inference and uncertainty quantification for medical image reconstruction with poisson data. *SIAM J. Imaging Sci.*, 13(1):29–52, 2020.